Title
Quantifying the effects of modeling uncertainty on the seismic performance assessment of a non-ductile reinforced concrete masonry-infilled frame structure

Author
Haindl, Mathias

Publication Date
2020

Peer reviewed|Thesis/dissertation

UNIVERSITY OF CALIFORNIA

Los Angeles

Quantifying the effects of modeling uncertainty on the seismic performance assessment of a non-ductile reinforced concrete masonry-infilled frame structure

A thesis submitted in partial satisfaction of the requirements for the degree Master of Science in Civil Engineering

by

Mathias Christian Haindl Carvallo

2020

ABSTRACT OF THE THESIS

Quantifying the effects of modeling uncertainty on the

seismic performance assessment of a non-ductile

reinforced concrete masonry-infilled frame structure

by

Mathias Christian Haindl Carvallo

Master of Science in Civil Engineering

University of California, Los Angeles, 2020

Professor Henry V. Burton, Chair

Quantifying and propagating aleatory and epistemic uncertainty in nonlinear structural response simulation is key to robust performance-based seismic assessments. In this thesis, the focus is on the probabilistic seismic performance assessment of a non-ductile three-story reinforced concrete infilled frame building. The uncertainty in ground motion records and the uncertainty embedded in structural model parameters are explicitly considered. An equivalent strut model is used for the masonry infill walls, where the six constitutive parameters that define its backbone curve are treated as random variables. The variability in these parameters is characterized by developing correlated and uncorrelated distributions of the deduced-to-predicted ratios using data from 113 experimental tests. The uncertainties are propagated using Latin hypercube sampling to generate randomized structural model realizations. Multiple stripe analysis is performed with hazard-consistent ground motions. The effect of considering modeling uncertainty is investigated in terms of the distributions of maximum story drift ratios and drift-based fragility functions. It is shown that the inclusion of modeling uncertainty has significant effects on the seismic performance of the case study building. The dispersion in the response and the mean annual frequency of exceeding the drift-based limit states are increased when modeling uncertainty is included. The initial stiffness of the infill walls is observed to have the most significant contribution to the performance of the building.

The thesis of Mathias Christian Haindl Carvallo is approved.

John Wright Wallace

Thomas A. Sabol

Henry V. Burton, Committee Chair

University of California, Los Angeles

2020

Contents

List of Figures

List of Tables

Chapter 1

Introduction

1.1 Motivation

Due to the shocking economic and social losses caused by severe earthquakes, structural and earthquake engineering has placed a large emphasis on whether the methodologies currently used for the design of structures achieve the desired performance.

In the last two decades, important efforts have been made to better understand earthquakes and their associated impacts on the performance of structural (Krawinkler & Deierlein, 2014).The invaluable scientific contribution to probabilistic seismic hazard assessment and the continuous development of cutting-edge technology has allowed a favorable evolution in seismic analysis of structures. The large amount of research and development of powerful and more efficient methodologies for structural analysis has made it possible to reliably understand and represent the behavior of diverse structural systems in diverse seismic scenarios. Performance-based earthquake engineering (PBEE) has emerged as a cornerstone methodology for predicting the behavior of structures under the action of earthquakes. Furthermore, due to the explicit consideration and quantification of the inherent variability associated with the stochastic nature of ground motions, and the uncertainties embedded in with modeling approaches used in structural analysis, the reliability of the seismic performance assessment of structures has been greatly enhanced. Regardless of these valuable scientific contribution and increasing advancements in modeling techniques, significant challenges remain to reliably characterize and quantify the behavior of structures (Gokkaya et al., 2020).

The analysis of structures is often conducted with deterministic models, which are intended to represent the mean or expected behavior of the structure. Under this assessment approach, if for example an incremental dynamic analysis (IDA) or multiple stripe analysis (MSA) is not performed, the effects of record-to-record and modeling uncertainties cannot be captured. While there have been several studies on quantification of uncertainties in performance-based analysis procedures, there are still important challenges ahead.

Non-ductile reinforced concrete masonry-infilled frame structures represent a type of contemporary structural system for which high levels of seismic vulnerability and sources of uncertainty can be recognized. This type of building is still being used for housing and industrial activities in many places around the world, although many were designed and built prior to the development of seismic design codes.

Reinforced concrete masonry-infill frame buildings, especially those where the lateral force resisting system consists of non-ductile frames, have suffered severe damage in past earthquakes. As a consequence, many efforts have been focused on understanding its seismic behavior and the main factors that determine its performance. Moreover, many experimental programs (Calvi et al., 2004; Morandi et al., 2014; Stavridis, 2009) have been conducted on this type of structural system, in which its highly nonlinear response under moderate seismic demands has been revealed, and significant sources of uncertainty have been recognized. The geometry of the masonry infill walls (i.e. with or without opening, height, length, etc.), the interaction between the masonry walls and the reinforced concrete (RC) frames under seismic forces, and the strength of masonry prism and mortar are only a few sources of the significant level of uncertainty embedded in this type of structural system. Therefore, it is crucial to strengthen the reliable identification, characterization, and communication of those uncertainties.

1.2 Previous research on modeling uncertainty quantification

While record-to-record uncertainty is routinely considered in PBEE assessments and its quantification is quite standardized, incorporation of modeling uncertainty has received less attention and is often difficult to quantify, mainly due to insufficient experimental data. The impacts of modeling uncertainty on the seismic performance of structures has been studied by several researchers. For instance, Liel et al. (2009) evaluated the methods of representing the uncertainty present in the modeling parameters and its impact on the collapse assessment process. Modeling uncertainty was considered for the parameters that define the constitutive behavior of the structural elements (level (ii) epistemic uncertainty according to Bradley, 2013). Different methods for incorporating the uncertainties are compared and its efficiencies and limitations are discussed. Jalayer et al. (2010) used an updated experimental database of RC structures to characterize the modeling uncertainty in material properties (level (i) epistemic uncertainty according to Bradley, 2013) and construction details. The authors proposed a Bayesian framework in order to update the probability distributions used for the modeling parameters. The study showed how the inclusion of modeling uncertainty increases both the mean and standard deviation of the demand to capacity ratio. Complementing this line of research, Gokkaya et al. (2017) quantified and examined the effects of modeling uncertainty on the drift demands and collapse capacity of different buildings. A framework was proposed to link the performance goals commonly present in building codes to specific acceptance criteria defined for each building.

Choudhury & Kaushik (2019) studied the treatment and quantification of uncertainties in the seismic fragility assessment of masonry-infilled RC frames. In this study, modeling uncertainty is considered at level (i) epistemic uncertainty. As infilled frame structures are not fully addressed in the building codes, an assessment of the effective uncertainty values proposed in the literature is conducted, indicating the limitations of using those values, and proposing alternative values to be used for different configurations of masonry-infilled frame structures.

Dolšek & Fajfar (2008) applied a simplified approach to the seismic performance assessment of three variants of reinforced concrete frame buildings. In terms of uncertainty quantification, this study was limited as it adopted defaults values for dispersion of modeling parameters and no explicit characterization was conducted. Using a different simplified procedure, Celarec & Dolšek (2013) evaluated the effect of epistemic uncertainty on the dispersion and median estimates of different response parameters by using the first-order-second-moment method. However, the reliability of this approach was shown to be limited, especially when the structural response is highly nonlinear.

There are few studies that have focused on modeling uncertainty at level (iii) and (iv) epistemic uncertainty (Bradley, 2013). Sattar et al. (2013) quantified the effect of modeling uncertainty on performance-based risk assessments, accounting for differences in software platforms, solution algorithm, element-types, and equations considered for model parameter calculations. A blind prediction contest was administered for an experimental evaluation of a 7-story RC building. The modeling uncertainty was quantified by comparing the predicted drift demands obtained from the different modeling approaches with the experimental results obtained from the full-scale test of the building. Although the aim of this study was to quantify the modeling uncertainty at level (iii), the authors recognized that more research is needed to understand the patterns of demand distributions and generalize, if possible, the observations to other structures.

1.3 Objectives

The main objectives of this thesis are to characterize and quantify the effect of the modeling uncertainties embedded in the backbone model used to represent the in-plane nonlinear behavior of masonry infill walls. Therefore, the aim of this study is to assess the effects of including record-to-record and modeling uncertainty on the seismic performance of an infilled frame structure.

To meet these objectives, multiple stripe analysis (MSA) is performed on a suite of randomized nonlinear model realizations generated by the Latin hypercube sampling (LHS) for three-story reinforced concrete masonry-infilled frame prototype building designed by Stavridis (2009). Modeling uncertainty is considered at the constitutive parameters level (Bradley, 2013). Hazard consistent-based selection of ground motions is considered at each hazard level assessed through MSA. Specifically, modeling uncertainty is considered for the six parameters that define the in-plane nonlinear behavior of the equivalent struts for representing the masonry infill walls (Huang et al., 2020). Based on a calibration procedure from existing experimental data of masonry-infilled RC frame systems, predictive equations were developed to compute the parameters that define backbone curve of the equivalent strut model. Thus, the modeling parameters associated with the equivalent strut model are considered as random variables. Quantification of modeling uncertainty at level (ii) (Bradley, 2013) is compared by using correlated and uncorrelated empirical and fitted distributions for the studied parameters. To differentiate the influence of record-to-record and modeling uncertainties, MSA is performed on a mean model of the structure (i.e. a model of the structure constructed using the mean values of the modeling parameters). The results of MSA allow the estimation of statistical parameters (median and standard deviation) and the construction of drift-exceedance fragility curves for the evaluation of the performance of the case study structure. Finally, given the site-specific seismic hazard considered for the prototype building, risk-based assessment is conducted and the mean annual frequency of exceed the desired limit states are given.

1.4 Organization

The focus of this thesis is on the characterization and quantification of the effects of modeling uncertainty embedded in the masonry infill strut model on the seismic performance of a reinforced concrete masonry-infilled frame structure. The organization of this document is as follows:

Chapter 2 presents an overview of the adopted methodology, followed by a description of the considered case study building, the modeling considerations for its analysis, and the seismic hazard-consistent ground motion selection procedure.

Chapter 3 provides a brief description of the sources of uncertainty and their treatments.The focus is on level (ii) epistemic uncertainty (i.e. uncertainty in the constitutive model parameters).

Chapter 4 describes the procedure used to characterize the modeling uncertainty and explains how it is propagated and quantified through the analysis and performance assessment of the structure.

Chapter 5 covers a detailed description of the case study building. Information about its geometry, material properties, and loads are given for analysis purposes. Additionally, record-to-record uncertainty is characterized by the definition of the hazard-consistent ground motion suites used to assess the seismic performance of the case study building.

Chapter 6 presents the results obtained from Multiple Stripe Analysis and the seismic performance assessment of the prototype building. Statistical distributions of the response demands are computed, and probabilities of exceeding the limit states associated with the masonry infill walls are provided.

Chapter 7 presents the main conclusions of this study. A summary of the key findings on uncertainty quantification and the limitations for the performance assessment of masonry-infilled RC frame structures are provided. Additionally, recommendations for future work are suggested.

Chapter 2

Overview of the methodology for uncertainty quantification

In this study, both the effects of the aleatory uncertainty associated with the natural randomness of ground motions (record-to-record uncertainty) and the epistemic uncertainty associated with model parameters (modeling uncertainty) are considered and quantified. In particular, level (ii) epistemic uncertainty according to Bradley (2013) is considered, which is associated with the parameters of the constitutive model used to simulate the nonlinear behavior of the masonry infill walls in a non-ductile reinforced concrete frame structure.

The strategy adopted to characterize and quantify the effects of the two sources of uncertainty on the seismic performance of the prototype building is based on a probabilistic analysis, in which MSA is performed for different hazard levels on nonlinear model realizations of the prototype building generated with LHS. Within this approach, hazard-consistent selection of ground motions is considered. For each model realization, eight ground motion records are randomly selected, each one representing one of the eight hazard levels. As a result, eight nonlinear analyses are performed on each model realization. To distinguish the effects of record-to-record uncertainty from modeling uncertainty, a separate analysis is performed on the mean model of the prototype building (i.e. a model constructed based on the mean values of the modeling parameters), for which the results represent the record-to-record component of uncertainty only. Using this model, the probability distribution parameters (median and dispersion) for the engineering demand parameters (EDPs) are estimated for each stripe analysis. Figure 2.1 summarizes the main steps of the methodology adopted to quantify the modeling uncertainty.

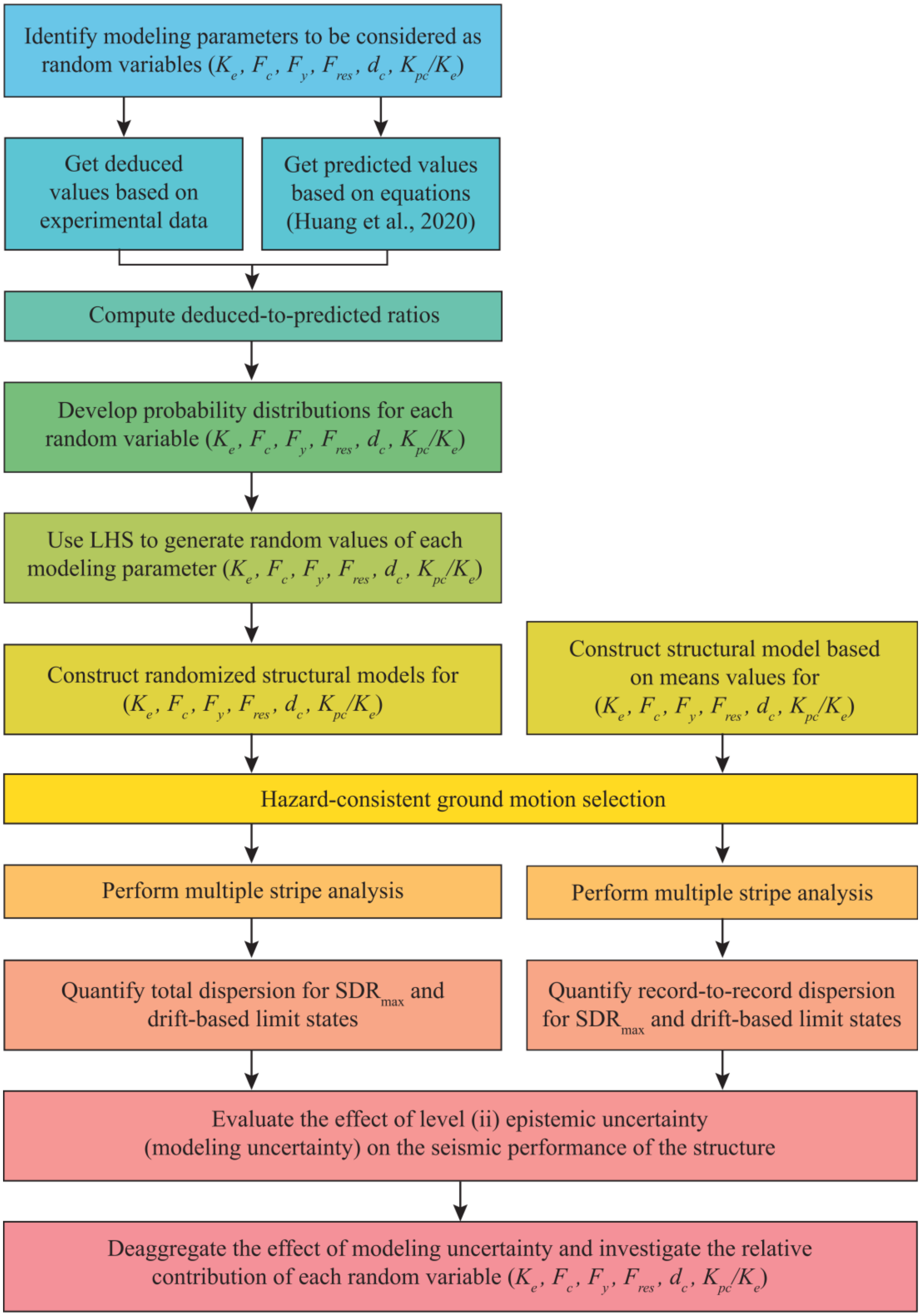

Figure 2.1 – Overview of methodology used to quantify the effects of modeling uncertainty

As illustrated in Figure 2.1, in this study, the maximum story drift ratio (SDR_{max}) is the primary EDP of interest since it is a good indicator of different limit states in this type of structure (Basha & Kaushik, 2016; Morandi et al., 2014; Stavridis et al., 2012). Modeling uncertainty is included and propagated using six constitutive modeling parameters as random variables. These constitutive modeling parameters define the shape of the backbone curve that governs the nonlinear in-plane axial behavior of the strut model used for the masonry infill walls (Huang et al., 2020). The probabilistic characterization of these parameters is carried out by representing each parameter of the strut's backbone curve model with statistical empirical and fitted continuous distributions.

Chapter 3

Treatment of uncertainties as part of the seismic performance assessment framework

It has been shown that the proper treatment of uncertainties is an essential step to enriching and improving the understanding of structural performance (Bradley, 2013; Liel et al., 2009). Different methodologies have been proposed to estimate the effects of uncertainties on the seismic performance of structures. Several authors have suggested frameworks for distinguishing these forms of uncertainty (Fox & Ulkumen, 2011). However, the quantification of uncertainties, especially epistemic, is still a major challenge in seismic performance and risk assessment.

In the seismic performance assessment framework, two main categories or dimensions of uncertainties are identified; the uncertainties resulting from the inherent variability in earthquake ground motions (aleatory), and the uncertainties that result from the lack of knowledge in the modeling assumptions use to predict the seismic behavior of a structural system (epistemic). The following sections briefly describe these two sources of uncertainty and its consideration as part of the seismic performance framework of this study.

3.1 Record-to-record uncertainty

Due to its largely stochastic nature, record-to-record uncertainty is considered a type of aleatory uncertainty. This form of uncertainty results from the inherent randomness in the frequency content of the ground motion records and has been widely studied and refined. In the performance-based assessment framework, record-to-record uncertainty is commonly taken into account by conducting nonlinear response history analysis (i.e. IDA, MSA, etc.) using a large enough number of ground motions records that are consistent with the seismic hazard at the site-location of the structural systems being analyzed (Bradley, 2013).

Figure 3.1 displays an example of a mean response spectrum that represents a single hazard level (stripe) characterized by a set of hazard-consistent ground motions, and the distributions of seismic responses caused by these ground motion in response history analysis.

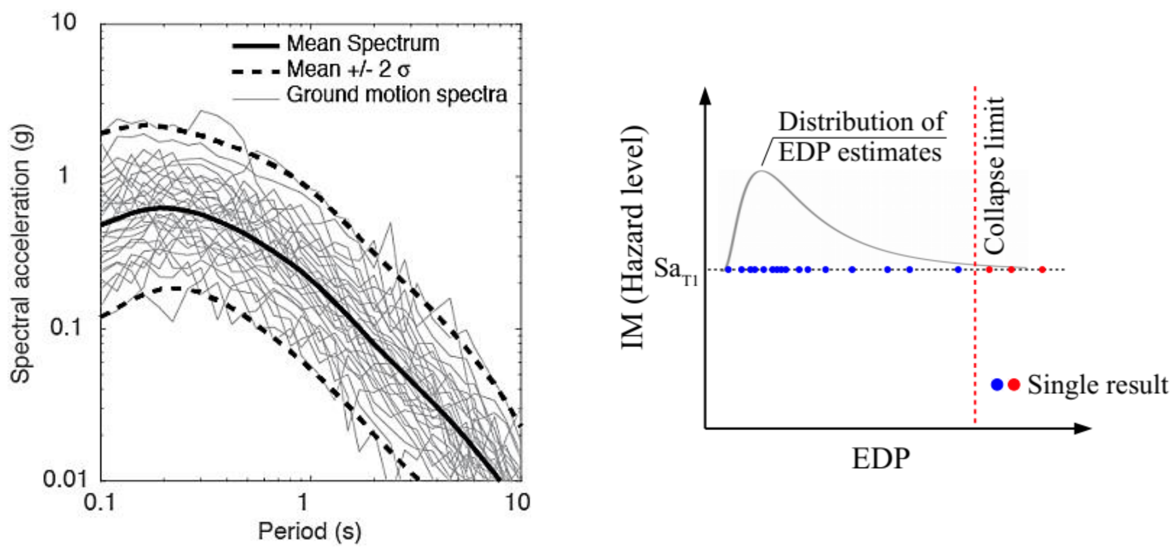

(a) (b)

Figure 3.1 – Example of (a) record-to-record variability on an unconditional spectra (Baker & Lee, 2018) and (b) results of a stripe analysis

It is worth noting that, although the quantification of record-to-record uncertainty is more often considered, there is still no standardized methodology, for example, to determine the optimal size of the ground motion ensemble to be used in the analysis (Bradley, 2013). In addition to record-to-record uncertainty, site-specific hazard curves constructed based on probabilistic seismic hazard analysis (PSHA) also account for the uncertainty embedded in the ground motion intensity by relating the spectral intensity to its probability of exceedance (Liel et al., 2009).

3.2 Modeling uncertainty

Modeling uncertainty has been increasingly studied by researchers in recent years, although still comparatively less than record-to-record uncertainty. However, regardless of the important contributions, the lack of experimental data and knowledge regarding many aspects of the seismic response of structural systems, has made the incorporation of modeling uncertainty a rather slow process and often difficult to quantify. Modeling uncertainty is normally represented as statistical distributions of a particular response parameter.

Bradley (2013), who has critically examined the consideration of the different sources of uncertainty within the performance assessment methodologies, disaggregated modeling uncertainty into four subcategories or levels. These levels are defined according to the degree of complexity, in ascending order, that is required for their consideration and quantification in the analysis. The four levels of modeling uncertainty are: (i) uncertainties in the characterization of basic parameters (e.g. mechanical properties of the structural materials, mass, loads, etc.); (ii) uncertainty in the relationships between the measured/observed physical quantities and the predicted constitutive modeling parameters (e.g. initial stiffness, yield strength, etc.); (iii) uncertainty in the chosen constitutive model to represent the behavior of structural components; and (iv) uncertainty in the assumptions and simplifications carried out in the model methodology (e.g. inability to capture all failure mechanisms). The assessment of the former two levels of modeling uncertainty has been increasingly considered in recent research, while the latter two are much less common due to the costly and time-consuming procedures.

Figure 3.2 depicts an example of a generic hysteretic backbone curve calibrated to represent the nonlinear behavior of masonry infill walls as an equivalent strut. Here, modeling uncertainty is considered at the constitutive parameter level (i.e. level (ii) epistemic uncertainty).

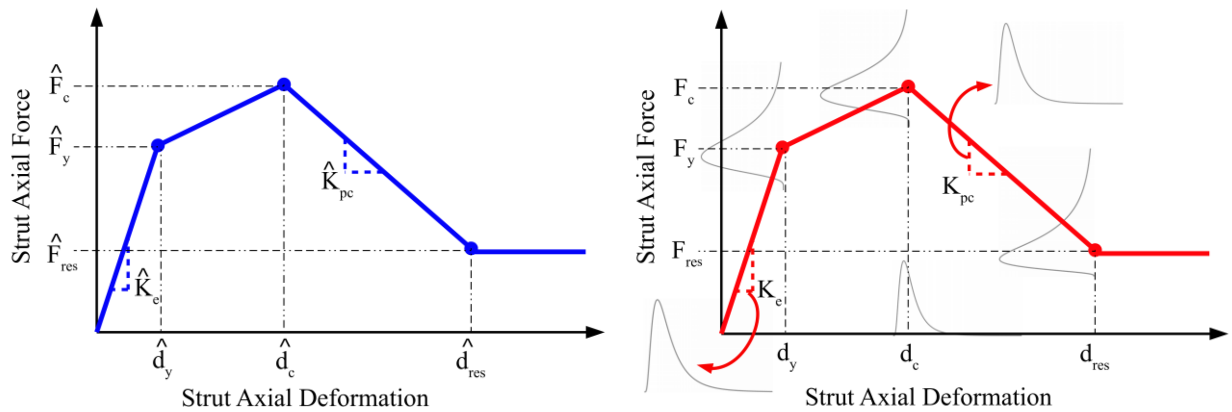

Figure 3.2 – Example of level (ii) epistemic uncertainty (modeling uncertainty) according to Bradley (2012); (a) mean model and (b) randomized model.

The propagation of modeling uncertainty through the analysis is commonly carried out by using nonlinear response history analyses, performed on several model realizations randomly generated based on the statistical distributions assumed for the randomized modeling parameters. In this regard, modeling uncertainty can be propagated in combination with record-to-record uncertainty.

It is important to note that, the description of uncertainties described here is not intended to be exhaustive, nor definitive. On the contrary, it serves as a global picture of a subset of uncertainties that are commonly recognized in structural analysis, thus highlighting the importance of quantifying them and evaluating their potential effects on seismic performance.

Chapter 4

Characterization of epistemic uncertainty for masonry infill strut model

The equivalent strut approach used to model masonry infill walls has been largely studied and refined (Holmes, 1961; Huang et al., 2020; Mehrabi et al., 1996; Stavridis, 2009; and others). This has enabled more reliable analyses and improved the understanding of the behavior of masonry infill walls as well as the enhancement of seismic performance assessment of reinforced concrete masonry-infilled frame structures. Recently, Huang et al. (2020) developed predictive equations for six modeling parameters that define the in-plane nonlinear axial behavior of the equivalent strut that represents the behavior of masonry infill walls in reinforced concrete frame buildings. These predictive equations were calibrated based on extensive research conducted on an experimental dataset of masonry-infilled systems, where regression analysis on a wide range of masonry-infilled systems was conducted. In this study, quantification of modeling uncertainty is focused on the uncertainties associated with the infill strut modeling parameters computed from the predictive equations proposed and developed by Huang et al. (2020).

The infill strut model is described by six modeling parameters; the initial stiffness (K_e); yield strength (F_y); capping strength (F_c) and the associated deformation (d_c); the residual strength (F_{res}); and the post-capping stiffness-to-initial stiffness ratio (K_{pc}/K_e). The proposed predictive equations to compute the infill strut modeling parameters are shown in Table 4.1.

Table 4.1 – Predictive equations for the parameters of the infill strut backbone model

Parameter	Predictive equation (Huang et al., 2020)	Determination coefficient (R^2)*	Residual standard error ($\hat{\sigma}$)*
K_e	$0.0143 \cdot E_m^{0.618} \cdot t_w^{0.694} \cdot \left(\frac{h_w}{l_w}\right)^{-1.096}$	0.54	0.56
F_c	$0.003766 \cdot f_m^{0.196} \cdot t_w^{0.867} \cdot l_d^{0.792}$	0.80	0.38
F_y	$0.72 \cdot F_c$	0.98	0.13
F_{res}	$0.4 \cdot F_c$	0.81	0.41
d_c	$0.0154 \cdot E_m^{-0.197} \cdot \left(\frac{h_w}{l_w}\right)^{0.978} \cdot l_d$	0.34	0.47
K_{pc}/K_e	$-1.278 \cdot f_m^{-0.357} \cdot t_w^{-0.517}$	0.32	0.46

* Based on the regression analysis conducted by Huang et al. (2020)

More details of the calibration process that was conducted for the development of the predictive equations and the model implementation can be reviewed in Huang et al. (2020).

To account for the variability and correlation in the each model parameter, statistical distributions for each parameter rely on the deduced parameters obtained from the experimental database and the values computed for each parameter based on the predictive equations. This way, the statistical distributions for each modeling parameter are developed by comparing the values of the modeling parameters deduced from the experimental results with the values calculated from the predictive equations (named here deduced-to-predicted ratios or errors). These deduced-to-predicted ratios represent a measure of the errors (ε) associated to the prediction of each modeling parameter value. Table 4.2 illustrates the procedure for computing the errors associated with each of the infill strut modeling parameters.

Table 4.2 – Computation procedure for errors (deduced-to-predicted ratios) associated with the infill strut modeling parameters

Specimen	Calibrated/Deduced value*	Predicted value**	Error (ε)***
1	d_1	p_1	$\frac{d_1}{p_1}$
2	d_2	p_2	$\frac{d_2}{p_2}$
3	d_3	p_3	$\frac{d_3}{p_3}$
⋮	⋮	⋮	⋮
N	d_N	p_N	$\frac{d_N}{p_N}$

* Deduced parameters from regression analysis conducted on the experimental dataset
** Predicted parameters computed from predictive equations (Huang et al., 2020)
*** Error (ε): Deduced-to-predicted ratios

Based on the computed errors, empirical and fitted probability distributions are defined for each model parameter of the strut. Kolmogorov–Smirnov test (K-S test) is used to evaluate the goodness-of-fit and decide whether the sample of computed errors follows a specific distribution (i.e. normal, lognormal, gamma, Rayleigh, etc.). After an iterative procedure, there is enough statistical evidence (at a 5% significance level) that the computed errors follow a lognormal distribution. Table 4.3 summarizes the statistical parameters of the distributions selected to describe the variability of each of the modeling parameters. It is worth mentioning that although the distributions are defined for the errors associated with the modeling parameters, each modeling parameter will follow the same corresponding distribution, since these are then multiplied only by a constant value (i.e. the predicted mean value of each parameter).

Table 4.3 – Distribution fitting for errors associated with infill strut backbone curve

Deduced-to-predicted ratio associated with	**Fitted distribution**	**K-S test p-value for 5% significance level**	**Probability parameters**
K_e	Truncated Lognormal	0.76	μ = -0.022, σ = 0.68 trunc = [0.22 , Inf [
F_c	Truncated Lognormal	0.93	μ = -0.017, σ = 0.49 trunc = [0.30 , Inf [
F_y	Truncated Lognormal	0.97	μ = -0.031, σ = 0.51 trunc = [0.25 , Inf [
F_{res}	Truncated Lognormal	0.33	μ = -0.008, σ = 0.78 trunc = [0.17 , Inf [
d_c	Truncated Lognormal	0.91	μ = -0.032, σ = 0.64 trunc = [0.17 , Inf [
K_{pc}/K_e	Truncated Lognormal	0.47	μ = -0.068, σ = 0.65 trunc = [0.13 , Inf [

To visualize the results listed in Table 4.3, Figure 4.1 demonstrates the fit between the empirical and the selected lognormal distributions for each strut model parameter.

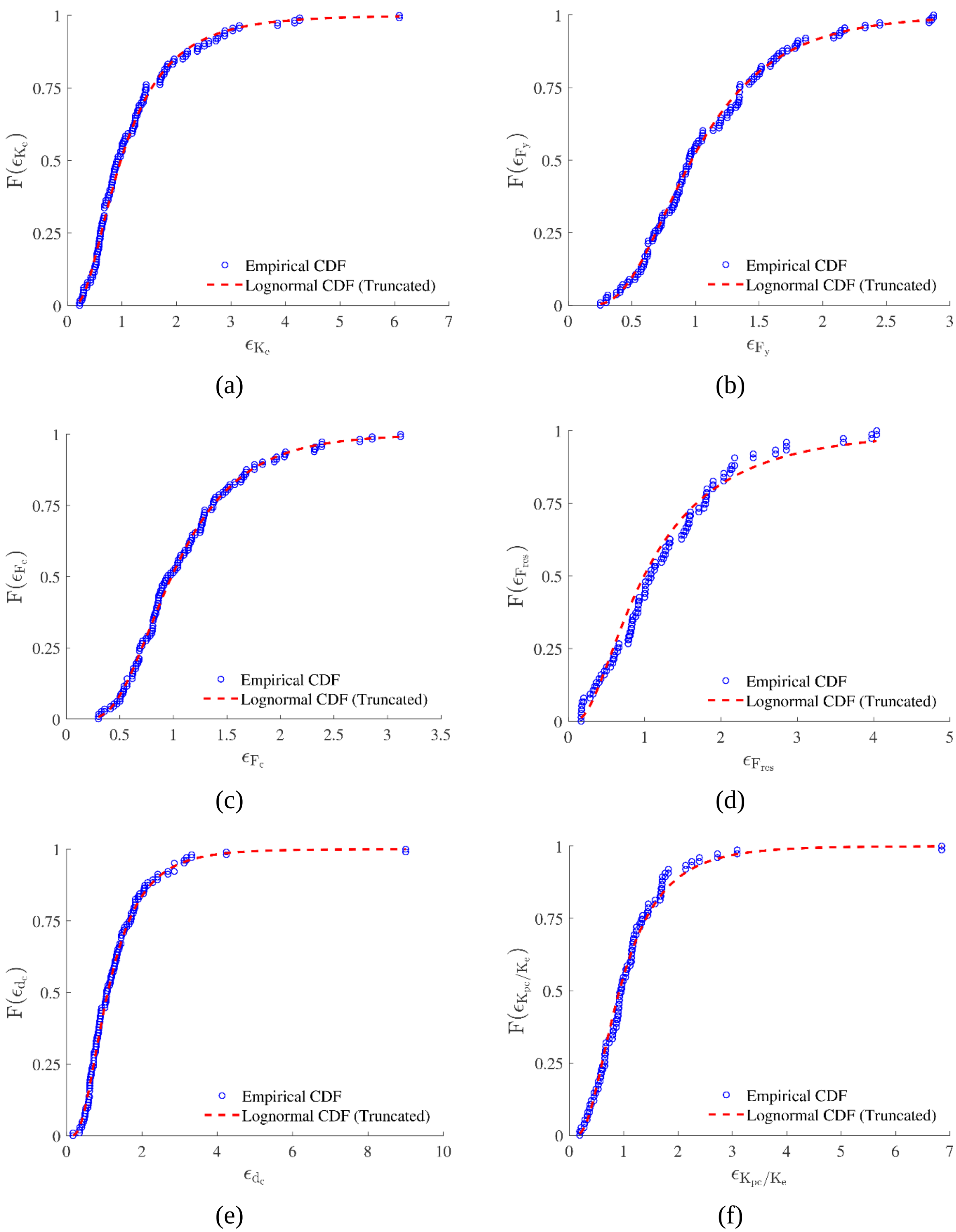

Figure 4.1 – Fit between empirical and the selected lognormal distributions for (a) K_e, (b) F_y, (c) F_c, (d) F_{res}, (e) d_c, and (f) K_{pc}/K_e

Figure 4.2 shows a schematic of the empirical and fitted truncated lognormal probability density functions (PDF) associated with each of the modeling parameters that define the backbone curve of the masonry infill struts.

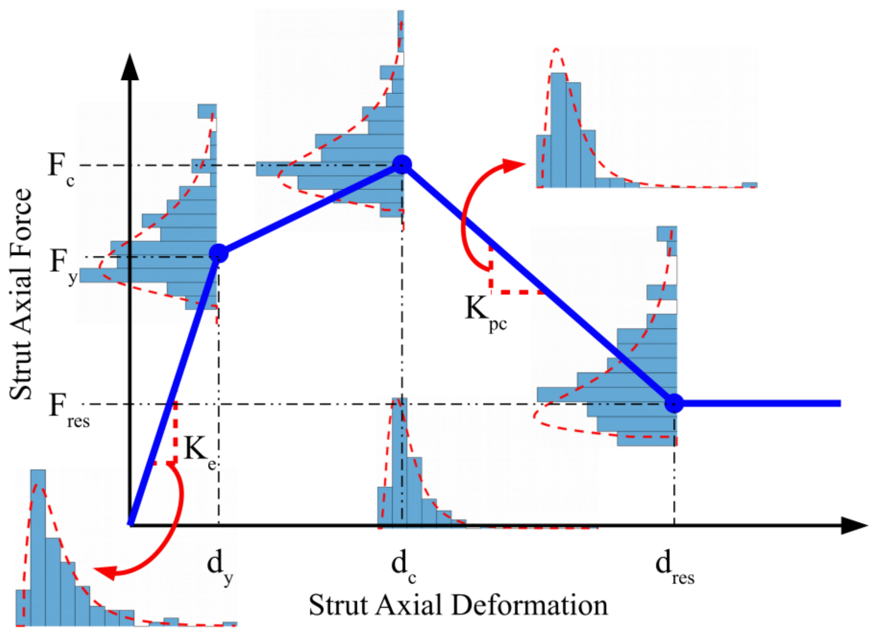

Figure 4.2 – Schematic of infill strut backbone curve with modeling parameters represented as empirical and fitted lognormal distributions

As part of the definition of the probability distributions for each modeling parameter, both correlated and uncorrelated parameters are considered. Therefore, correlated and uncorrelated empirical and fitted distributions, respectively, are used to sample and construct the nonlinear model realizations. This way, the influence of accounting for correlation in the infill strut modeling parameters is assessed. The correlation coefficients computed for the infill strut modeling parameters is displayed in Table 4.4.

Table 4.4 – Correlation coefficients for the errors (Ɛ, deduced-to-predicted ratios) associated with the infill strut model parameters

		Parameter error					
		ε_{K_e}	ε_{F_c}	ε_{F_y}	$\varepsilon_{F_{res}}$	ε_{d_c}	ε_{K_{pc}/K_e}
Parameter error	ε_{K_e}	1.00	0.71	0.61	0.55	-0.35	-0.12
	ε_{F_c}		1.00	0.93	0.81	-0.18	0.07
	ε_{F_y}			1.00	0.79	-0.17	0.01
	$\varepsilon_{F_{res}}$				1.00	-0.26	-0.06
	ε_{d_c}		Sym.			1.00	0.17
	ε_{K_{pc}/K_e}						1.00

As mentioned before, only the parameters that define the infill strut backbone curve (Huang et al., 2020) are considered as correlated/uncorrelated random variables in this study. Moreover, structural elements are treated as independent for correlation purposes, i.e. no explicit correlation is assumed between modeling parameters of different structural elements.

Finally, to quantify and propagate the modeling uncertainty through the performance analysis, Latin Hypercube Sampling (LHS) is conducted. As discussed in many studies (Ugurhan et al., 2013; Vamvatsikos & Fragiadakis, 2010; Vořechovský & Novák, 2003; Dolšek, 2009), LHS has been demonstrated to be an effective method in the process of sampling random variables with and without correlation. By stratification of the probability function that defines the distribution of a random variable, the number of simulations is considerably reduced compared to other techniques such as Monte Carlo simulation (Dolšek, 2012). In this study, by examining the convergence of the results from the performance assessment analysis in terms of median (Θ) and dispersion (β) values for maximum story drifts, 500 model realizations of the strut modeling parameters are generated based on LHS method. Additionally, each model realization is randomly combined with eight ground motions, each representing one of defined seismic hazard-consistent levels.

Figure 4.3 shows an example of the backbone curve for the mean model and the curves generated for fifty model realizations. Finally, Figure 4.4 summarizes the procedure used to determine the set of structural models for the four variants of analysis (i.e. empirical with correlation (E_C), empirical without correlation (E_{NC}), fitted distribution with correlation (F_C), and fitted distribution without correlation (F_{NC})).

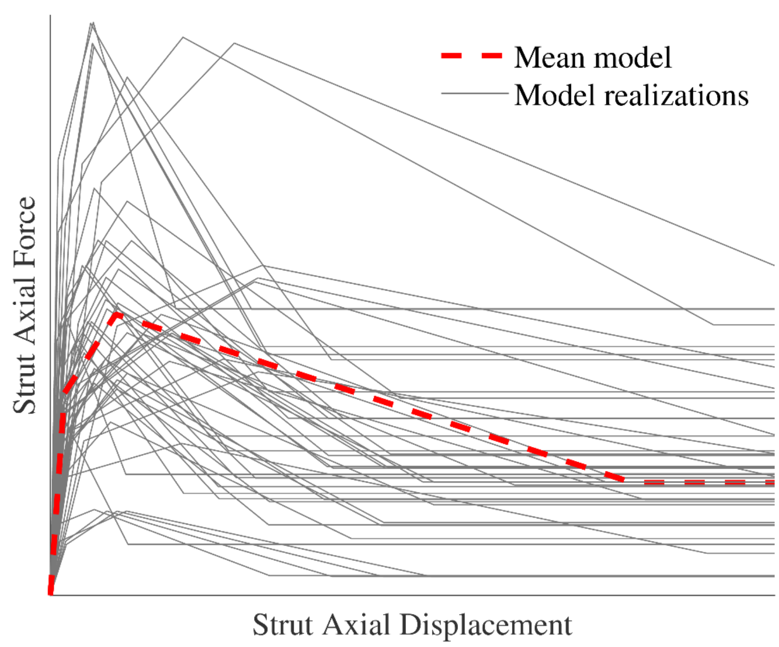

Figure 4.3 – Example of strut backbone curves generated with LHS

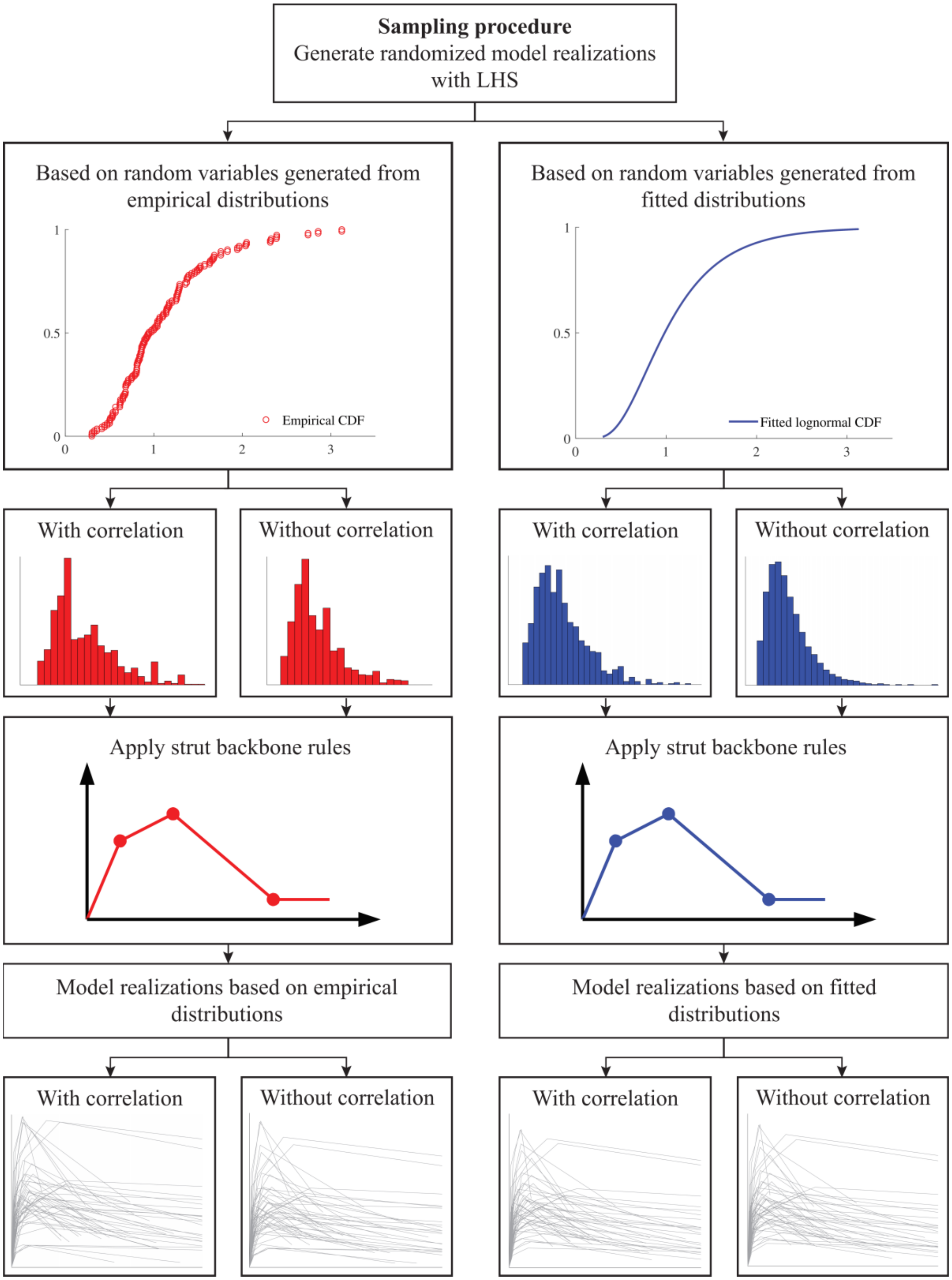

Figure 4.4 – Sampling procedure for the different variants of analysis

Chapter 5

Case study: Reinforced concrete masonry-infilled frame structure

The previously described methodology for the quantification of both record-to-record and modeling uncertainties is applied to the study case prototype building designed and studied by Stavridis (2009). The prototype building consists of a three-story non-ductile reinforced concrete frame structure with unreinforced three-wythe masonry infill walls. This type of building represents a common construction practice in the 1920s era in California. However, masonry-infilled RC frames with similar design details as the prototype building analyzed in this study are still often used for housing and industrial activities in many parts of the world. Furthermore, this type of structure continues to be a common construction practice in places where the seismic hazard is considered a great concern.

5.1 Prototype building

The three-story non-ductile reinforced concrete frame prototype building is assumed to be located in the Los Angeles area, California. The site specific coordinates in latitude and longitude are 34.208 and -118.604, respectively.

Based on ASCE 7 (American Society of Civil Engineers, 2017) seismic categorization, a risk category II (based on occupation activity) and site class D (Vs_{30} = 259 m/s) are considered. The basic spectral parameters S_S and S_1 at the maximum considered earthquake (MCE) level are determined as 1.5 and 0.6g, respectively, which was also considered by Stavridis & Shing (2015). Additionally, the fundamental period for the undamaged condition of the building, for 5% damping ratio, is estimated as 0.1 seconds, which is consistent with the fundamental period obtained from modal analysis of the prototype building in Open System for Earthquake Engineering Simulation (OpenSees, McKenna et al., 2000). More detailed information about the design of the prototype building is given in Stavridis (2009).

5.1.1 Geometry

A three-dimensional, plan, and elevation views of the prototype building with its global dimensions is shown in Figure 5.1. The masonry infill walls located in the perimeter reinforced concrete frames consist of three-wythe brick masonry walls. For the purposes of this research, the masonry infill walls are considered as fully solid walls, i.e. without any openings.

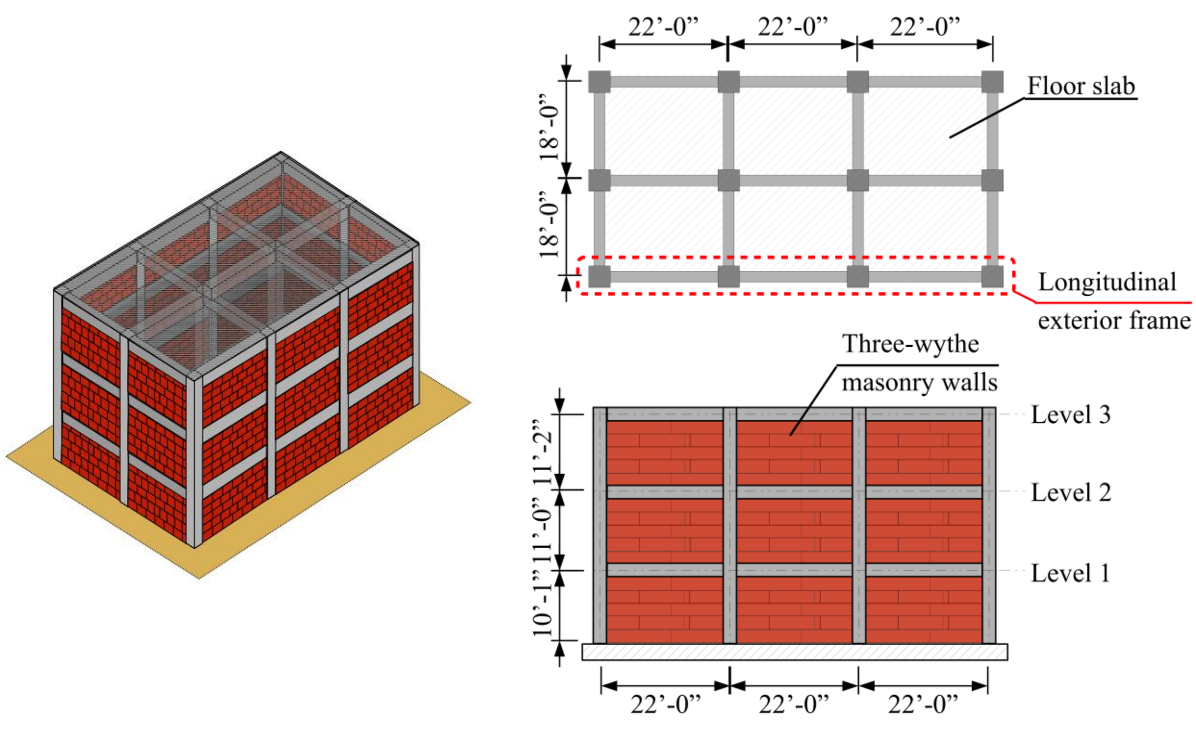

Figure 5.1 – 3D scheme of the prototype building, plan view, and elevation of longitudinal exterior frame with global dimensions.

The lateral force resisting system corresponds to the perimeter frames, where the masonry infill walls are located. Interior columns and beams are considered as gravity-only structural components. Floor system corresponds to a reinforced concrete thin slab supported by joists in the longitudinal direction of the structure. Figure 5.2 shows an elevation view of the analyzed three-bay-three-story longitudinal frame with design details of beams and columns. Additionally, Table 5.1 summarizes the design details for those structural components.

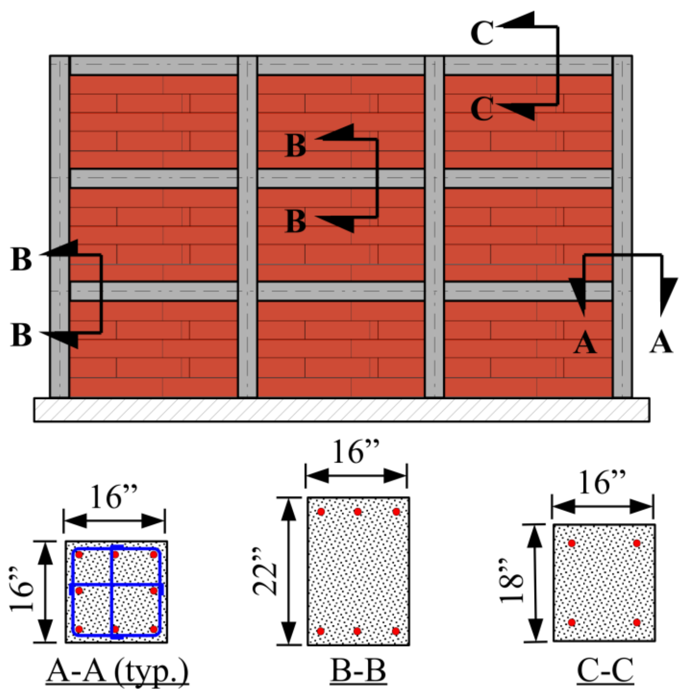

Figure 5.2 – Elevation view of the longitudinal exterior frame and structural component details

Table 5.1 – Design details of the reinforced concrete frame structural components

	Story level	Width (in.)	Depth (in.)	Bottom reinf.	Top reinf.	Stirrups
Beam design	1	16	22	3#8	3#7	NO
	2	16	22	3#8	3#7	NO
	3 (roof)	16	18	2#8	2#6	NO
Column design	**Story level**	**Width (in.)**	**Depth (in.)**	**Vertical reinf.**		**Stirrups**
	1	16	16	8#7		#3@16”
	2	16	16	8#6		#3@16”
	3 (roof)	16	16	8#5		#3@16”

5.1.2 Material properties

Concrete beams and columns were modeled with compression strength f_c’ = 5.75 [ksi] and modulus of elasticity E_c = 2395 [ksi]. Reinforcement bars were considered with strength at yield f_y = 62.5 [ksi] and a modulus of elasticity E_s = 29000 [ksi].

The compression strength and modulus of elasticity for the masonry prism was considered as f_m = 3.2 [ksi] and E_m = 906.5 [ksi], respectively. These correspond to measured mean values, which were obtained through an extensive test program conducted on the materials used for the construction of the prototype building. More details are provided in Stavridis & Shing (2015).

5.1.3 Loads

The seismic weight of the prototype building is estimated as 755 [kips] (Stavridis & Shing, 2015). Since in this study the analysis is conducted on half the lateral resisting system in the longitudinal direction, the seismic weight is taken as 372 [kips]. Additionally, Table 5.2 lists the components that contribute to the building weight and loads as reported in Stavridis (2009), where more details about the configuration and the structural design of the prototype building can be reviewed.

Table 5.2 – Loads considered for the analysis of the longitudinal exterior frame

Component	Units	Level 1 and 2	Level 3 (roof)
Topping	psf	12.5	5
Ceiling	psf	12	12
Mechanical equipment	psf	N/A	5
Infill panels	pcf	130	N/A
Parapet	lbs/ft	N/A	390
Live loads	psf	75	20

5.2 Structural model

Giving the symmetry of the prototype building, the seismic performance assessment is conducted through a two-dimensional model that accounts for the lateral force resisting system in the longitudinal direction of the building. Therefore, a two-dimensional nonlinear structural model was developed using OpenSees. Rayleigh damping based on the first and third modal frequencies is used for the dynamic analysis with 5% critical damping. Figure 5.3 schematically illustrates the modeling approach used for the longitudinal masonry-infilled frame.

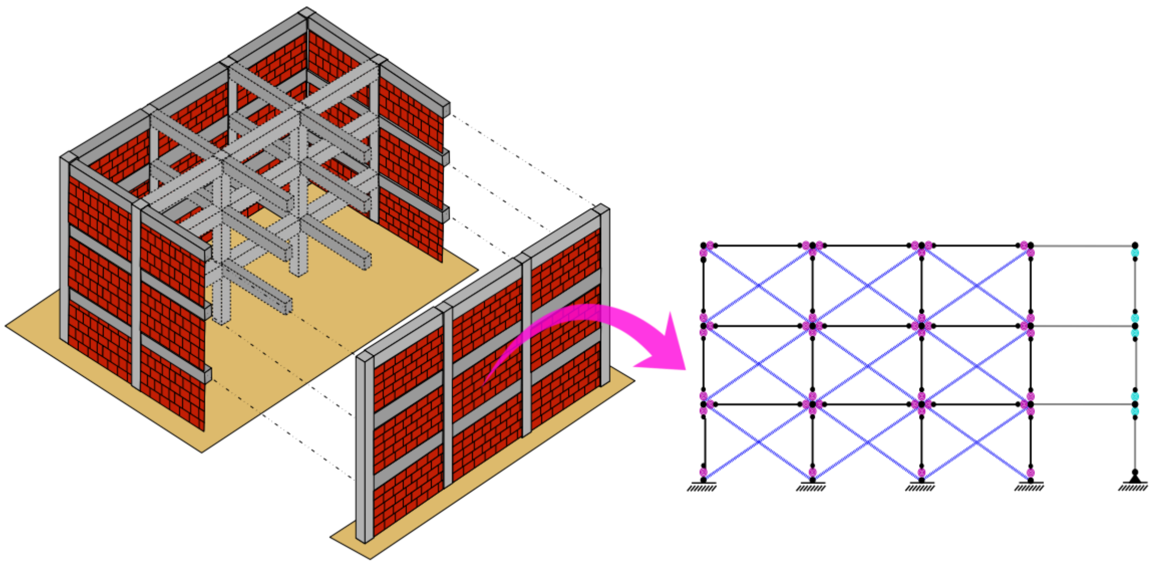

Figure 5.3 – Schematic modeling approach for the longitudinal exterior RC frame with masonry infill panels (note that floor slabs are not shown)

As illustrated in Figure 5.3, leaning columns are connected by rigid trusses to the RC frame system at each floor level. Rotational springs with very small stiffness are considered at the ends of the leaning columns to avoid incorporating additional flexural stiffness. Leaning columns are used to represent the P-Delta effects caused by half the portion of the gravity load resisted by the interior columns of the prototype building. Figure 5.4 shows a more detailed scheme of the configuration of the numerical model developed in OpenSees.

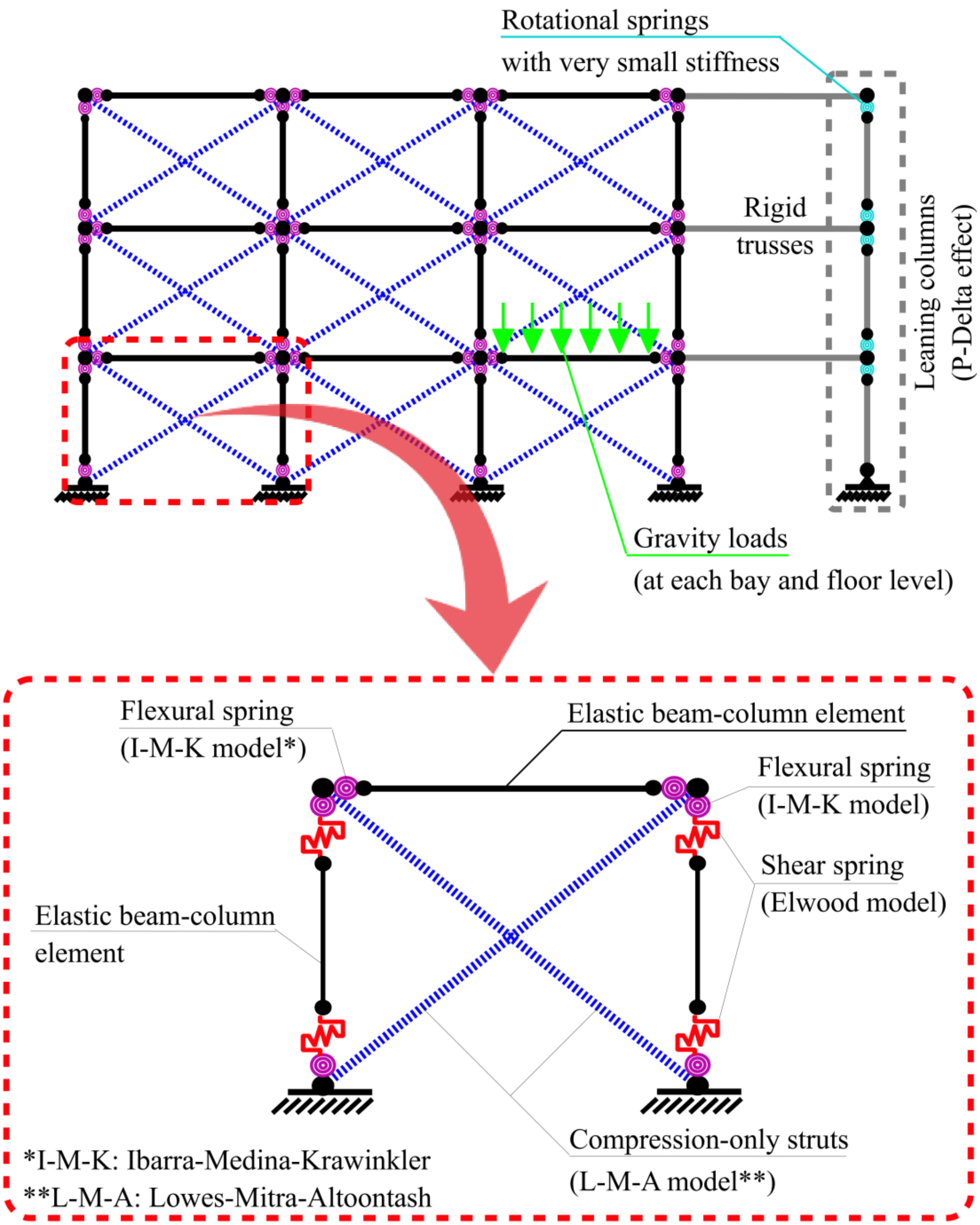

Figure 5.4 – Schematic configuration of two-dimensional nonlinear model of the prototype building constructed in OpenSees

A concentrated plasticity model is considered for the connection of the reinforced concrete elements, i.e. beams and columns. As described in Huang et al. (2020), the frame structural components are modeled as elastic elements with flexural moment-rotation (M-Θ) springs/hinges at its ends. The semi-empirical equations calibrated by Haselton et al. (2016) are used to determine the parameters that define the hysteretic behavior of those flexural hinges and the Ibarra-Medina-Krawinkler (I-M-K) model (Ibarra et al., 2005) is incorporated. Additionally, according to the model developed by Elwood (2004), shear failure of columns is considered by adding a shear hinge in series with the flexural hinge at each column ends. Dimensions at centerlines of the frame elements are considered for modeling the RC frame system.

The masonry infill walls are modeled as two compression-only diagonal struts using a truss element with the Lowes-Mitra-Altoontash (Lowes et al., 2003) pinching material model (Pinching4 material in OpenSees). The modeling parameters that define the backbone curve for the axial behavior of the equivalent strut are computed from the predictive equations developed by (Huang et al., 2020, see Chapter 4). These parameters are the initial stiffness (K_e), yield strength (F_y), capping strength (F_c) and the associated deformation (d_c), residual strength (F_{res}), and the post-capping stiffness-to-initial stiffness ratio (K_{pc}/K_e). The Lowes-Mitra-Altoontash model is adopted since it gives more adaptability in terms of backbone shape and cycling degradation effects to represent the infill strut hysteretic behavior. Figure 5.5 shows the axial force-displacement relationship that defines the infill strut model.

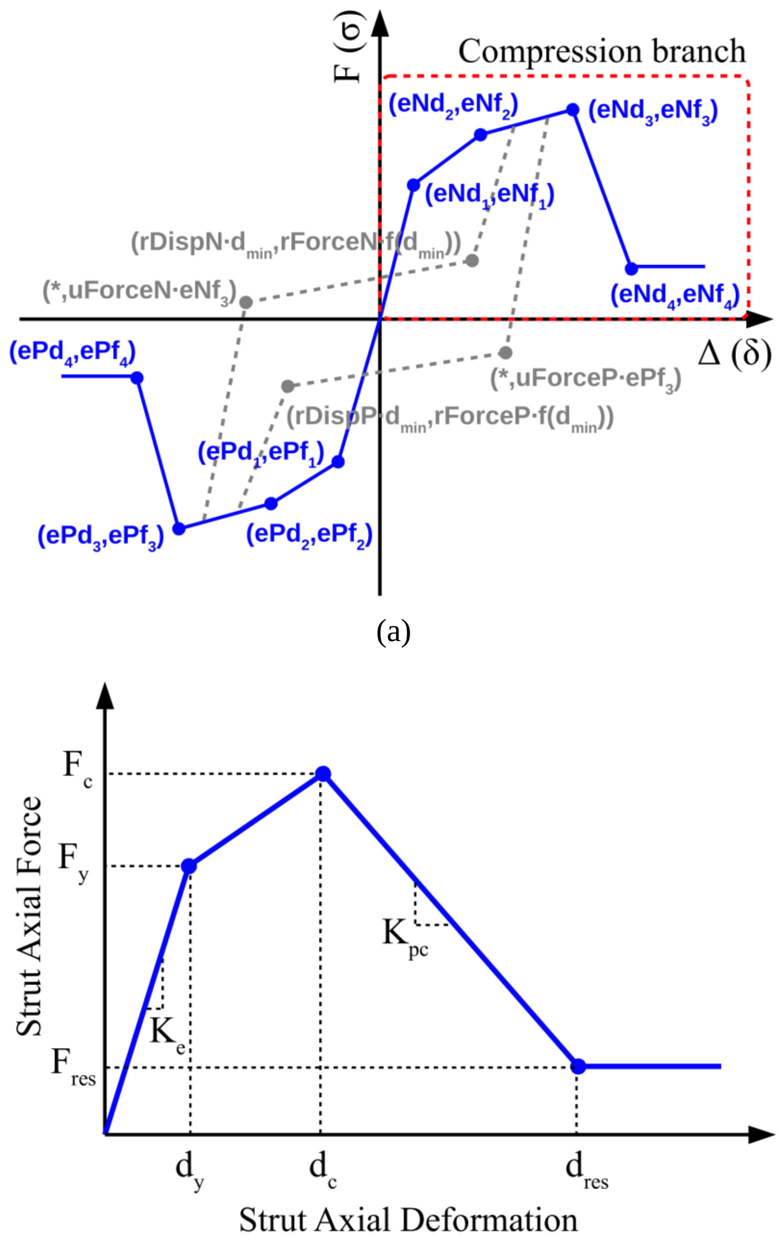

Figure 5.5 – (a) Lowes-Mitra-Altoontash model and (b) axial force-displacement relationship for the strut model

Since the infill strut model considers compression-only action, the parameters that define the tension branch of the hysteretic curve are assumed to be almost zero in order to avoid numerical issues during the analysis. The relationship between the infill strut backbone curve parameters defined by the Huang et al. (2020) model and the Lowes-Mitra-Altoontash (L-M-A) response model is represented in Table 5.3.

Table 5.3 – Relationship between the infill strut backbone parameters and those of the Lowes-Mitra-Altoontash (L-M-A) model

Backbone parameter	Calibrated L-M-A model parameters
K_e	$\frac{eNf_1}{eNd_1 \cdot l_d}$
F_y	eNf_1
F_c	eNf_3
d_c	$eNd_3 \cdot l_d$
K_{pc}	$\frac{eNf_4 - eNf_3}{(eNd_4 - eNd_3) \cdot l_d}$
F_{res}	eNf_4

As stated in Huang et al. (2020) a unit strut area is used in the axial response of the equivalent strut so the calibrated stress is the same as the associated force. Mean values are used for the cyclic degradation and pinching parameters. Mean values are also used for the mass, loads, damping ratio, and properties used to define the modeling parameters for the RC elements (i.e. beams and columns). Based on the geometry and measured mean values of the mechanical properties of materials, the computed predicted mean values for the six modeling parameters of the infill strut model are listed in Table 5.4.

Table 5.4 – Mean values computed for the Lowes-Mitra-Altoontash model used for the equivalent struts

Modeling parameter	Units	Story level 1	Story level 2	Story level 3
K_e	kip/in	2235.2	2235.2	2149.4
F_c	kip	242.2	245.3	245.9
F_y	kip	174.4	176.6	177.0
F_{res}	kip	96.9	98.1	98.4
d_c	in	0.36	0.37	0.38
K_{pc}	kip/in	-50.8	-50.8	-48.9

For simplicity, the structural model does not consider the contribution in stiffness and strength on the beams provided by the concrete floor slab at each story level. The possibility of foundation uplift is also not considered, which means that the bases of the columns are modeled as fixed.

5.3 Hazard-consistent ground motion selection

The prototype building site (34.208 and -118.604) in Los Angeles, California, is used for the hazard-consistent ground motion selection. In the hazard analysis and ground motion selection procedure, the information required is obtained from the Unified Hazard Tool provided online[1] by

[1] https://earthquake.usgs.gov/hazards/interactive/

The United States Geological Survey (U.S. Geological Survey, 2020). This tool allows users to obtain the target spectral accelerations at the fundamental period of the structure (Sa_{T1}) for different hazard levels. Furthermore, disaggregation information about the sources that contributes to the site hazard is also retrieved using the USGS tool.

Here, it is assumed that the spectral acceleration at the fundamental period of the prototype structure in the direction of analysis and its site location are the main parameters needed for ground motion selection (Krawinkler et al., 2003). Based on Site Class D and spectral acceleration at 0.1 seconds, which is estimated as the fundamental period of the prototype structure, eight hazard levels are selected. These hazard levels are ranged from 20% to 0.5% probability of exceedance in 50 years. Selected suites of 80 (40 pairs) hazard-consistent ground motions are considered for each hazard level, in which the mean spectra reasonably match the target spectra derived from ground motion models (GMMs) in the region of interest. Table 5.5 summarizes the information for each selected hazard and the disaggregation parameters (m: magnitude, r: rupture distance, and epsilon ($\mathcal{E}_o$): number of standard deviations that separates the mean logarithmic spectral acceleration and the observed spectral acceleration based on calculations made by using the GMMs (Baker & Cornell, 2006).

Table 5.5 – Hazard-consistent ground motion intensities considered for performance assessment

Hazard level	Return period (years)	Probability of exceedance (in 50 years)	Target PSa_{T1} (g)	m*	r*	ε_o*
1	72	50%	0.43	6.33	18.23	0.66σ
2	224	20%	0.71	6.42	14.93	1.27σ
3	475	10%	0.92	6.47	13.43	1.63σ
4	975	5%	1.15	6.51	12.16	1.94σ
5	2475	2%	1.51	6.61	10.96	2.31σ
6	5000	1%	1.81	6.71	10.24	2.57σ
7	7500	0.7%	2.01	6.76	9.51	2.70σ
8	10000	0.5%	2.16	6.76	8.06	2.74σ

*Values for Campbell & Bozorgnia (2014) GMM (CB14)

The mean target spectra at each hazard level is computed as the average of the spectra obtained from the Campbell & Bozorgnia (2014), Abrahamson, Kamai & Silva (2014), and Chiou & Youngs (2014) GMMs. From the USGS disaggregation tool, the mean site-specific values, i.e. magnitude, rupture distance, and epsilon (ε_o), are obtained for each of the designated GMMs. This way, the site-specific unconditional spectra (i.e. not conditioned on a spectral value) are defined for the analysis and seismic performance assessment of the prototype building. Figure 5.6 depicts the response spectra for the eight sets of ground motions corresponding to each of the hazard levels.

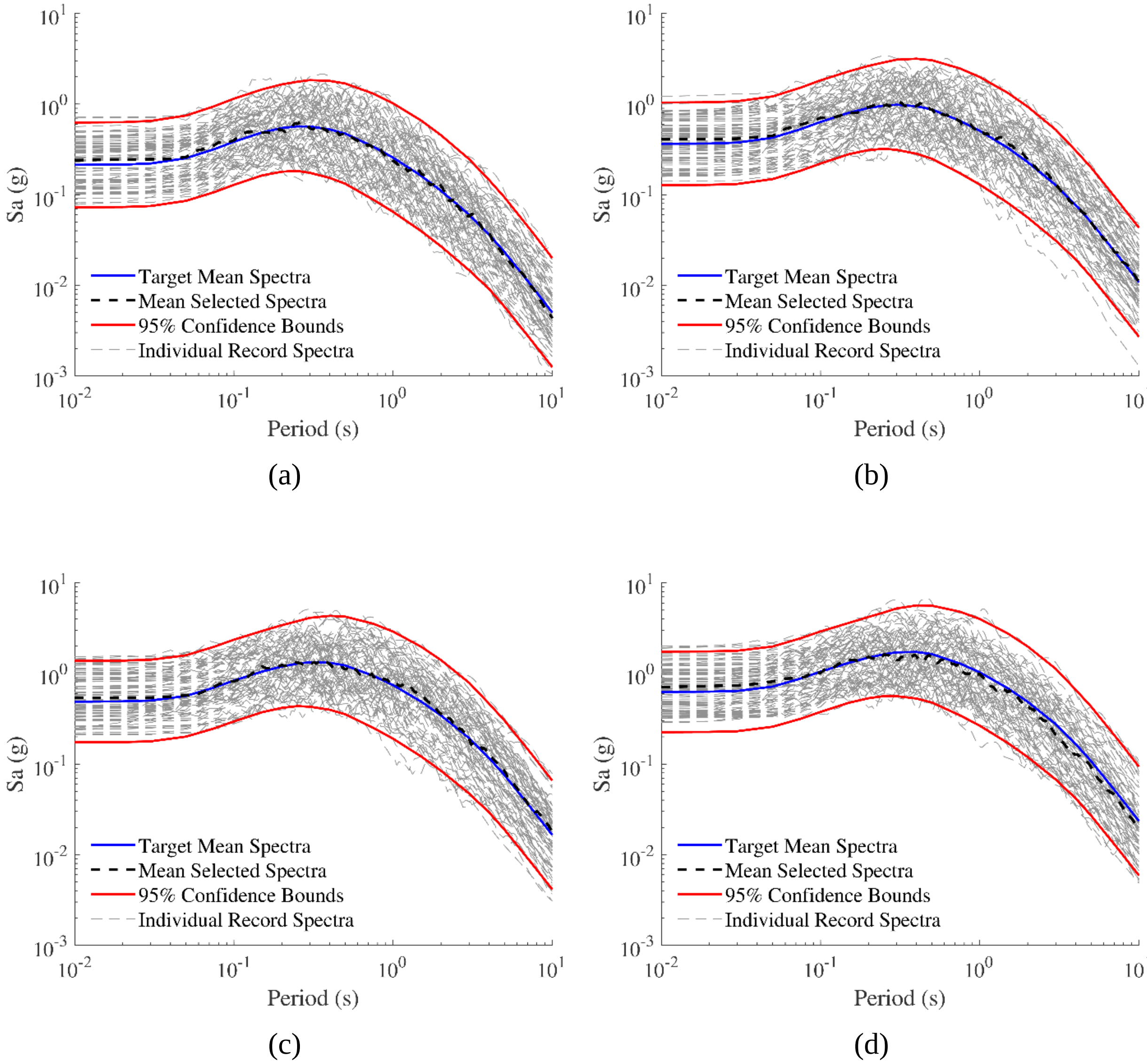

Figure 5.6 – Response spectra for selected suites of ground motions corresponding to (a) 50%, (b) 20%, (c) 10%, (d) 5%, (e) 2%, (f) 1%, (g) 0.7%, and (h) 0.5% in 50 years, respectively

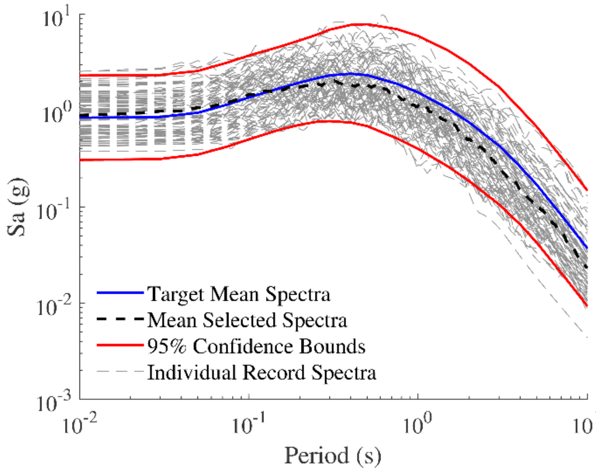

(e)

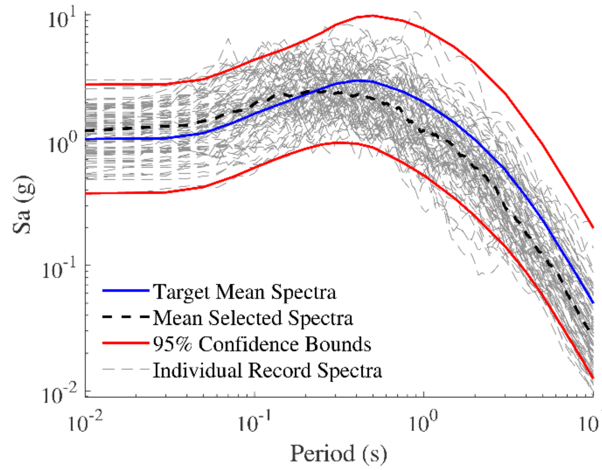

(f)

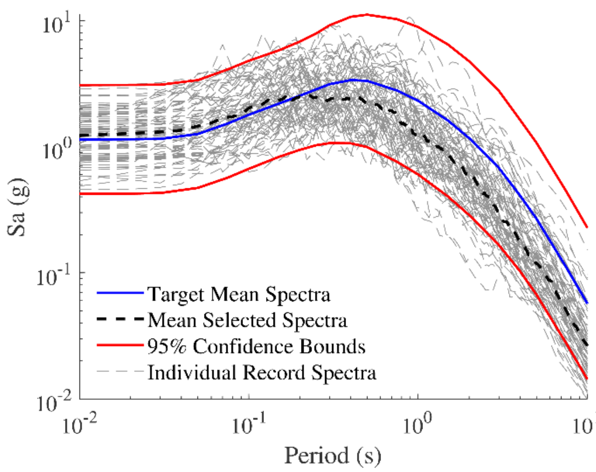

(g)

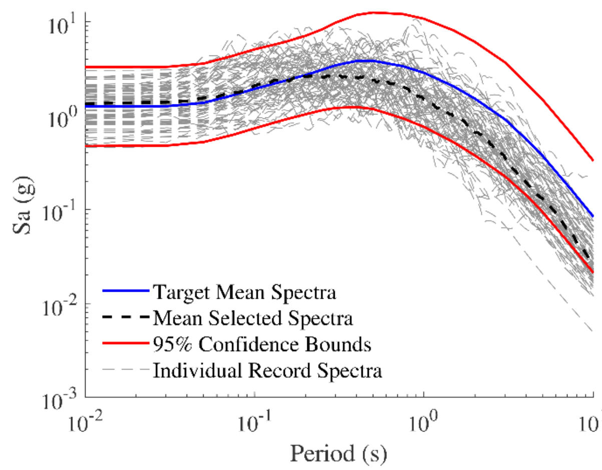

(h)

Figure 5.6 (continued) – Response spectra for selected suites of ground motions corresponding to (a) 50%, (b) 20%, (c) 10%, (d) 5%, (e) 2%, (f) 1%, (g) 0.7%, and (h) 0.5% in 50 years, respectively

A maximum scale factor of 3.0 was considered for the selection of the hazard-consistent suites of ground motions. Additionally, based on probabilistic seismic hazard analysis (PHSA), and given the site location of the prototype building and its estimated fundamental period, the period-dependent hazard curve is also obtained from the USGS Uniform Hazard Tool. Figure 5.7 shows the hazard curve corresponding to the fundamental period of the case study structure.

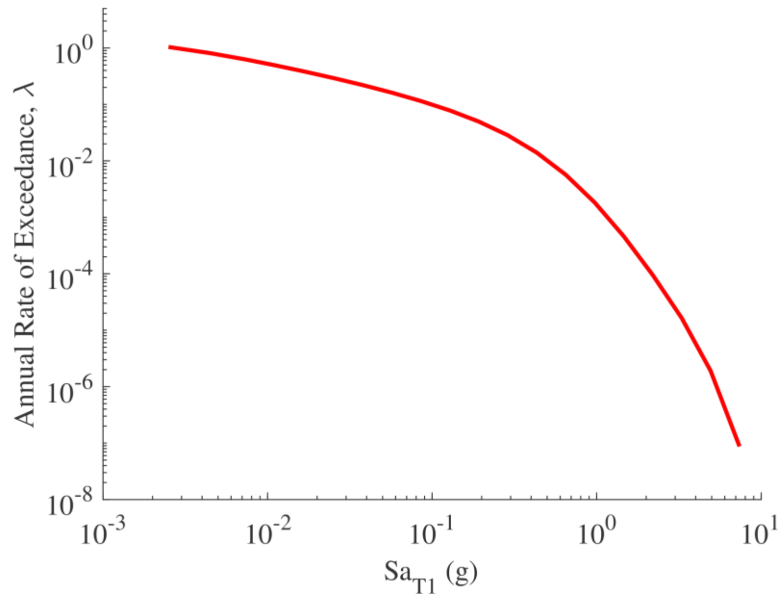

Figure 5.7 – Period-dependent hazard curve for T_1 = 0.1 sec.

5.4 Definition of limit states for performance assessment

The SDR_{max} is the EDP to assess the seismic performance of the prototype structure and examine the effects of modeling uncertainty. Five drift-based limit states (LSs) are defined corresponding to 0.25%, 0.7%, 1.5%, 3%, and 5% SDR_{max}. According to previous studies conducted on these type of structural systems (Basha & Kaushik, 2016; Masi, 2003; Stavridis, 2009; Stavridis & Shing, 2015), Table 5.6 lists the selected drift limit states and the associated failure patterns.

Table 5.6 – Definition of drift limit states for seismic performance assessment

Drift-based limit state	**Associated failure pattern**	**Reference**
0.25%	Diagonal/sliding shear cracking of masonry infill wall	Stavridis & Shing (2015)
0.7%	Structure lateral strength reduced to 80% of peak strength	From pushover curve (this study)
1.5%	Collapse of masonry infill wall	Stavridis & Shing (2015) Masi (2003)
3%	Severe damage on RC frame system (shear failure predominantly)	Stavridis (2009) Basha & Kaushik (2016)
5%	Global collapse of the structure	Basha & Kaushik (2016)

Seismic performance is assessed through drift-exceedance fragility curves generated in terms of the spectral acceleration at the fundamental period of the structure normalized by the reference spectral acceleration at the maximum considered earthquake (MCE) level ($Sa_{T1,MCE}$ = 1.51 [g]).

Chapter 6

Seismic performance assessment with modeling uncertainty

The mean model and the four variants of probabilistic models (i.e. considering empirical and fitted probability distribution for the strut modeling parameters, and with and without correlation, respectively) outlined in Chapter 4, are used to assess the seismic performance of the prototype building. In order to estimate EDP distributions at the different hazard levels, and quantify record-to-record and modeling uncertainties, MSA is conducted over the mean and randomized structural models, respectively, for the predefined set of hazard levels.

Statistical measures (median and dispersion) for the selected EDP (i.e. maximum story drift ratio) are presented, and drift-exceedance fragility curves are generated in order to conduct a risk-based assessment of the prototype building. Furthermore, differences among the variants of analysis are noted and deaggregation of modeling uncertainty effects is presented.

6.1 Effects of modeling uncertainty on maximum story drift demands

For each model realization, one ground motion record is randomly selected for each of the eight hazard levels. This results in eight nonlinear response history analyses performed on each model realization. From the empirical distributions of SDR_{max} obtained at each hazard level, the statistical median and dispersion are first computed for the mean model (i.e. a model constructed based on the mean values of the modeling parameters), which allows us to isolate the effects of record-to-record uncertainty (RTR). Then, these results are compared against the results obtained by including modeling uncertainty (total uncertainty: TOT) according to the procedure described in Chapter 4.

6.1.1 Drift-response considering record-to-record uncertainty only

MSA is performed on the structural model constructed based on the mean values of the modeling parameters (mean model hereinafter) (see Table 5.4) to quantify the record-to-record uncertainty. Figure 6.1 shows the results of the MSA, where empirical responses for SDR_{max} are represented in the form of "stripes", with each one corresponding to one of the hazard levels.

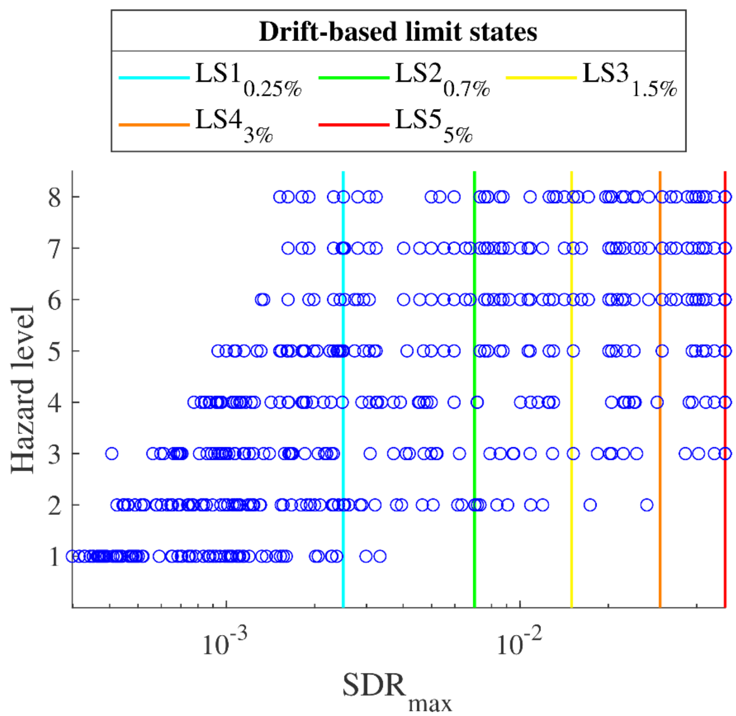

Figure 6.1 – Results of MSA for the mean model of the prototype structure

Each "stripe" (hazard level) is composed by a total of 80 responses, which correspond to the SDR_{max} obtained from each nonlinear response history analysis. It is worth noting that MSA is performed for a different set of ground motion records at each hazard level. Additionally, as it is shown in Figure 6.1 an SDR_{max} of 0.05 is assumed for the collapse threshold.

The median and dispersion measures obtained from the MSA for SDR_{max} by considering record-to-record uncertainty only are summarized in Table 6.1.

Table 6.1 – Median and dispersion measures of SDR_{max} for record-to-record uncertainty

Hazard level	**$\theta_{SDR,RTR}$ (%)**		**$\beta_{SDR,RTR}$**		**Collapse cases (% of total analyses)**
	*	**	*	**	
1	0.07	0.07	0.61	0.64	0.0
2	0.15	0.11	0.99	1.07	0.0
3	0.25	0.22	1.21	1.89	13.8
4	0.34	0.38	1.24	1.95	17.5
5	0.47	0.97	1.16	2.03	30.0
6	0.98	2.10	1.03	1.62	31.3
7	1.00	2.51	0.98	1.50	36.3
8	1.17	3.79	1.02	1.34	42.5

* Parameters computed based on "non-collapse" cases with lognormal distribution

** Parameters computed based on counted median and fractional standard deviation

To estimate the demand parameters (i.e. θ and β), a lognormal distribution is fitted to the SDR_{max} responses. Two methods for representing their distributions are used; by considering the non-collapse cases results only (i.e. cases that reach convergence during the analysis and/or resulted in an SDR_{max} less than 5%); and by computing the counted median and fractional standard deviation of the total responses (including collapse cases), at each hazard level respectively. Counted median is considered as the 50th percentile of the responses, while the fractional standard deviation is estimated as the mean value between lognormal value of the 84th over the 50th

percentile and the lognormal value of the 50th over the 16th percentiles. These approaches to estimating the parameters based on non-collapse demands and counting has been largely utilized, mainly to avoid issues of bias that could be introduced by non-convergence and collapse cases (Jalayer & Cornell, 2009). Moreover, the assumption that the demands follow a lognormal distribution may no longer be valid when too many collapse are observed.

As observed from Table 6.1, when only record-to-record uncertainty is considered, the median SDR_{max} increases with the hazard levels. At the equivalent MCE level (2% probability of exceedance in 50 years according to ASCE 7) the median SDR_{max} is increased 1.16 times. These results suggest that the structure is susceptible to significant cracking at the masonry infill walls (70% probability of exceeding the 0.25% drift threshold). Moreover, the probability of exceeding the limit state for collapse is 17.5%, which highlights the high vulnerability of this building. For the observed non-collapse cases, the median SDR_{max} is increased 16.5 times from hazard level 1 to hazard level 8.

Dispersion in SDR_{max} due to record-to-record uncertainty is observed to increase up to the hazard level with 975 years return period, which is consistent with the trend observed for the median SDR_{max} and the increasing nonlinear behavior due to damages on the infill walls. However, for higher ground motion intensities, the dispersion on SDR_{max} starts to decrease, which is likely a result of the change in the number of collapse cases, or near-collapse cases, where the distribution of demands no longer follows a lognormal distribution.

6.1.2 Drift-response including the effects of modeling uncertainty

To account for and propagate the modeling uncertainty through the analysis, MSA is performed on 500 model realizations constructed through LHS. As noted in Chapter 4, sampling is based on the developed empirical and fitted distributions for the infill strut modeling parameters, with and without correlations. Figure 6.2 shows the response "stripes" with the distributions for SDR_{max} obtained from MSA, where the total uncertainty (i.e. combined record-to-record and modeling uncertainty) is considered.

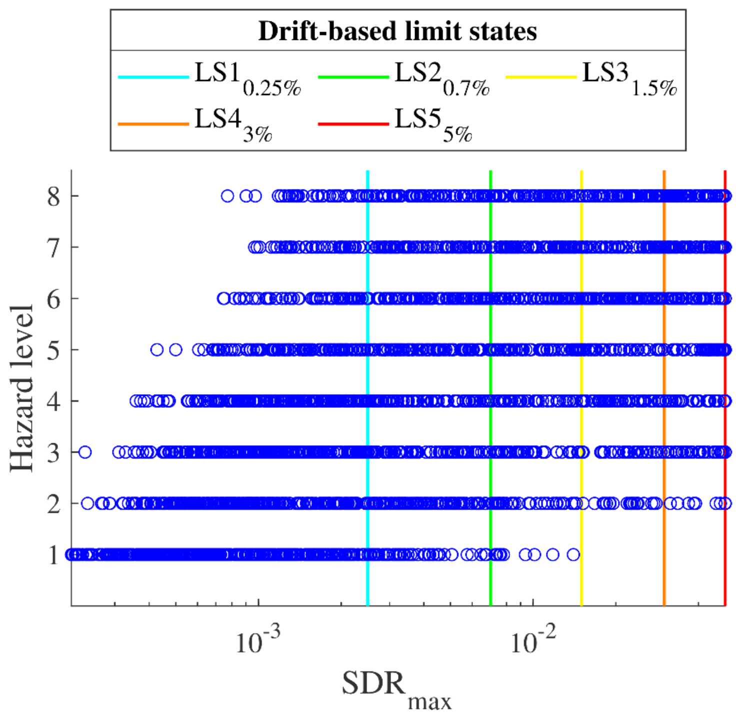

Figure 6.2 – Results of MSA for the model realizations of the prototype structure

Figure 6.2 shows the SDR_{max} responses obtained for the analysis in which modeling parameters are sampled based on the correlated empirical distributions (E_C). Based on these results shown in Figure 6.2, Table 6.2 and Table 6.3 summarize the statistical median and dispersion measures for the four variants of analysis.

Table 6.2 – Median values of SDR_{max} with inclusion of modeling uncertainty

Hazard level	**$\theta_{SDR,TOT}$ (%) E_C[1]**		**$\theta_{SDR,TOT}$ (%) E_{NC}[2]**		**$\theta_{SDR,TOT}$ (%) F_C[3]**		**$\theta_{SDR,TOT}$ (%) F_{NC}[4]**		**Collapse cases (% of total analyses) (A[1]/B[2]/C[3]/D[4])**
	*	**	*	**	*	**	*	**	
1	0.08	0.07	0.09	0.07	0.09	0.07	0.08	0.07	0.0/0.0/0.0/0.0
2	0.18	0.15	0.18	0.14	0.17	0.14	0.16	0.13	2.0/1.2/2.0/0.8
3	0.28	0.26	0.28	0.26	0.27	0.24	0.26	0.25	9.2/10.6/8.6/ 11.8
4	0.34	0.37	0.40	0.44	0.35	0.39	0.37	0.38	13.6/11.4/16.0/13.8
5	0.54	0.97	0.51	1.00	0.53	1.06	0.53	1.11	25.4/26.8/27.4/26.0
6	0.84	1.77	0.85	1.79	0.80	1.80	0.85	1.72	26.8/29.0/29.2/25.4
7	0.85	1.83	0.88	2.32	0.90	2.41	0.97	2.16	30.2/32.4/33.8/30.2
8	0.97	2.43	0.98	2.76	1.04	2.95	1.05	2.66	35.4/38.4/37.6/34.8

[1] E_C: Using empirical distribution with correlation

[2] E_{NC}: Using empirical distribution without correlation

[3] F_C: Using fitted distribution with correlation

[4] F_{NC}: Using fitted distribution without correlation

* Parameters computed based on "non-collapse" cases (SDR_{max} < 5%)

** Parameters computed based counted median and fractional standard deviation

Table 6.3 – Dispersion measures of SDR_{max} with inclusion of modeling uncertainty

Hazard level	**$\beta_{SDR,TOT}$ E_C[1]**		**$\beta_{SDR,TOT}$ E_{NC}[2]**		**$\beta_{SDR,TOT}$ F_C[3]**		**$\beta_{SDR,TOT}$ F_{NC}[4]**	
	*	**	*	**	*	**	*	**
1	0.82	0.80	0.85	0.84	0.83	0.82	0.82	0.79
2	1.09	1.21	1.19	1.29	1.14	1.20	1.09	1.10
3	1.24	1.60	1.29	1.78	1.31	1.77	1.21	1.77
4	1.22	1.81	1.28	1.71	1.29	1.91	1.23	1.83
5	1.17	1.96	1.16	2.03	1.21	2.00	1.22	2.04
6	1.10	1.71	1.09	1.69	1.09	1.76	1.09	1.69
7	1.07	1.70	1.07	1.59	1.09	1.70	1.08	1.65
8	1.07	1.58	1.13	1.71	1.06	1.56	1.10	1.59

[1] E_C: Using empirical distribution with correlation

[2] E_{NC}: Using empirical distribution without correlation

[3] F_C: Using fitted distribution with correlation

[4] F_{NC}: Using fitted distribution without correlation

* Parameters computed based on “non-collapse” cases

** Parameters computed based on full stripe results

The results shown in Table 6.2 and Table 6.3 are graphically visualized in Figure 6.3, which shows plots of the median versus dispersion ratios computed as the quotient between the results obtained from the analysis with record-to-record uncertainty and total uncertainty, respectively.

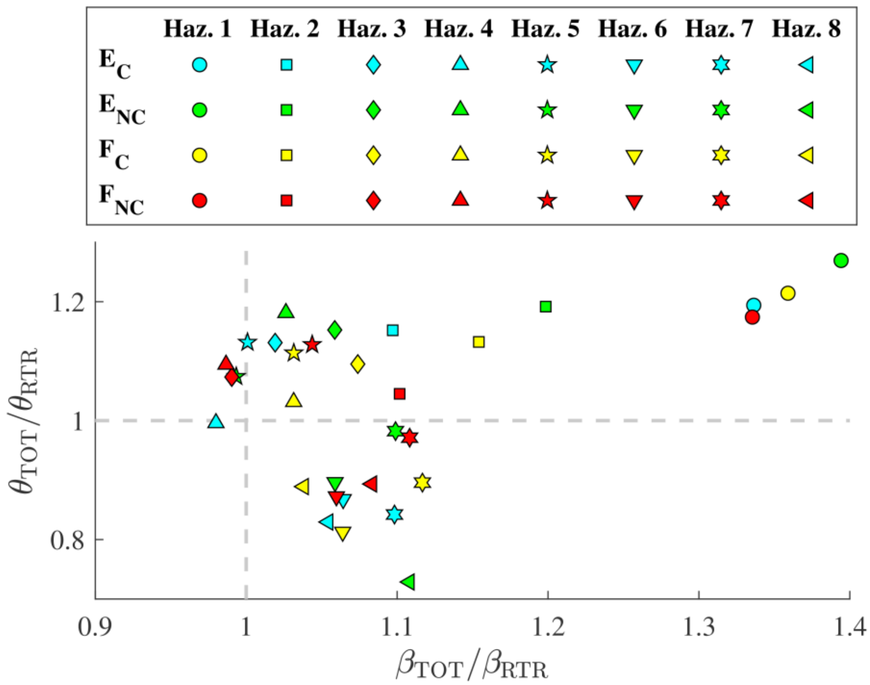

Figure 6.3 – Change in median versus change in dispersion of SDR_{max} at each hazard level due to the inclusion of modeling uncertainty (referred to the distribution of the non-collapse cases)

In general, the change in median and dispersion ($\Theta_{TOT}/\Theta_{RTR}$ and β_{TOT}/β_{RTR}) are similar when they are computed based on the non-collapse and the counted values. The non-collapse cases approach results in slightly higher values for the change in dispersions, while the counted approach results in marginally higher values for the change in the medians.

As reflected in Figure 6.3, the inclusion modeling uncertainty increases the dispersion in almost all the analysis variants and hazard levels. On average, the dispersion increases 10% due to the inclusion of modeling uncertainty. A few exceptions can be identified for hazard levels 3, 4, and 5, for which the dispersion decreases with respect to the case with record-to-record uncertainty only. These exceptions are for the results obtained from the analysis performed on model realizations where the modeling parameters are sampled from correlated empirical distributions (cyan colored symbols) and with uncorrelated fitted distributions (red colored symbols), respectively. Dispersion has its maximum increase for hazard level 1, in which the increase is on average 35%, and shows a decreasing trend for higher levels, reaching to a 7% increase for the 0.5% probability of exceedance in 50 years hazard. It is worth mentioning that the dispersion observed in hazard level 1 seems to be very high since at this hazard level the structure is supposed to have not experienced much nonlinearity. Furthermore, the higher impact on median SDR_{max} is observed when modeling parameters are sampled from uncorrelated empirical distributions. The median SDR_{max} increases on average 18% for the first five hazard levels, and shows a decrease by 15% for the three most severe intensities.

At the hazard level with 2% probability of exceedance in 50 years (hazard level 5), the median SDR_{max} is 0.47% based on the mean value of the non-collapse cases (i.e. with exclusion of collapse cases) of the four variants of analysis. This result is 12.2% higher than the median SDR_{max} computed for the same hazard level with consideration of record-to-record uncertainty only. The same trend is observed for dispersion, where it increases by 2.5% when modeling uncertainty is included.

6.2 Drift-exceedance fragility assessment

Drift-exceedance fragility curves are generated based on the results obtained from the MSA for the five aforementioned limits states. At each hazard level, the probability of exceeding each limit state is computed as the fraction of ground motions that resulted in SDR_{max} greater than the value defined for each limit state (see Table 5.6). The drift-exceedance fragility curves are represented by parameterized lognormal distributions (Baker, 2015). The maximum likelihood method is implemented to generate the corresponding drift-exceedance fragility curves.

6.2.1 Fragility curves considering only record-to-record uncertainty

Figure 6.4 shows the fragility curves when only record-to-record uncertainty is considered. The curves are shown in terms of spectral acceleration at the fundamental period of the structure (Sa_{T1}), normalized with respect to the spectral acceleration at the hazard level with 2% probability of exceedance in 50 years (S_{MT}), versus probability of exceed the limit state.

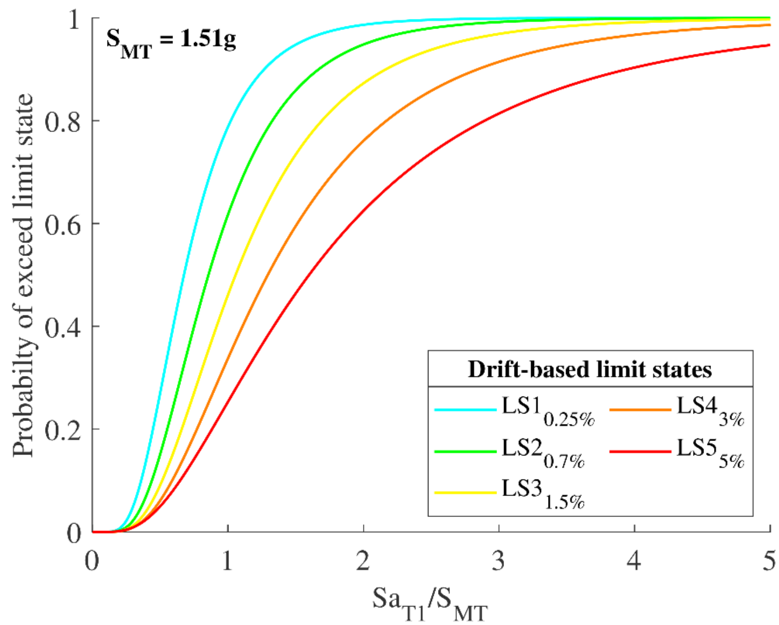

Figure 6.4 – Drift-exceedance fragility curves with consideration of record-to-record uncertainty only

Table 6.4 summarizes the fragility function parameters (median and dispersion) at each limit state, computed based on maximum likelihood fitting technique.

Table 6.4 – Fragility function parameters for record-to-record uncertainty only

Drift-based limit state	$\theta_{SaT1,RTR}$	$\beta_{SaT1,RTR}$
0.25%	1.02	0.49
0.7%	1.29	0.52
1.5%	1.59	0.56
3%	1.96	0.61
5%	2.41	0.70

According to the fragility parameters shown in Table 6.4, a clear increase of both the median and dispersion is observed, which is consistent with the higher demands associated with the more severe limit states. The dispersion of the fragility functions ranges from 0.49 to 0.7, while the median intensity (not normalized) ranges from 1.02 [g] at the first limit state (0.25% drift threshold) to 2.41 [g] at the most severe limit state (5% drift threshold). The median represents the spectral acceleration for which 50% of the cases are expected to observe an SDR_{max} greater than value corresponding to the limit state threshold.

6.2.2 Fragility curves considering the effects modeling uncertainty

Figure 6.5 shows the change in the drift-exceedance fragility curves due to the consideration of modeling uncertainty.

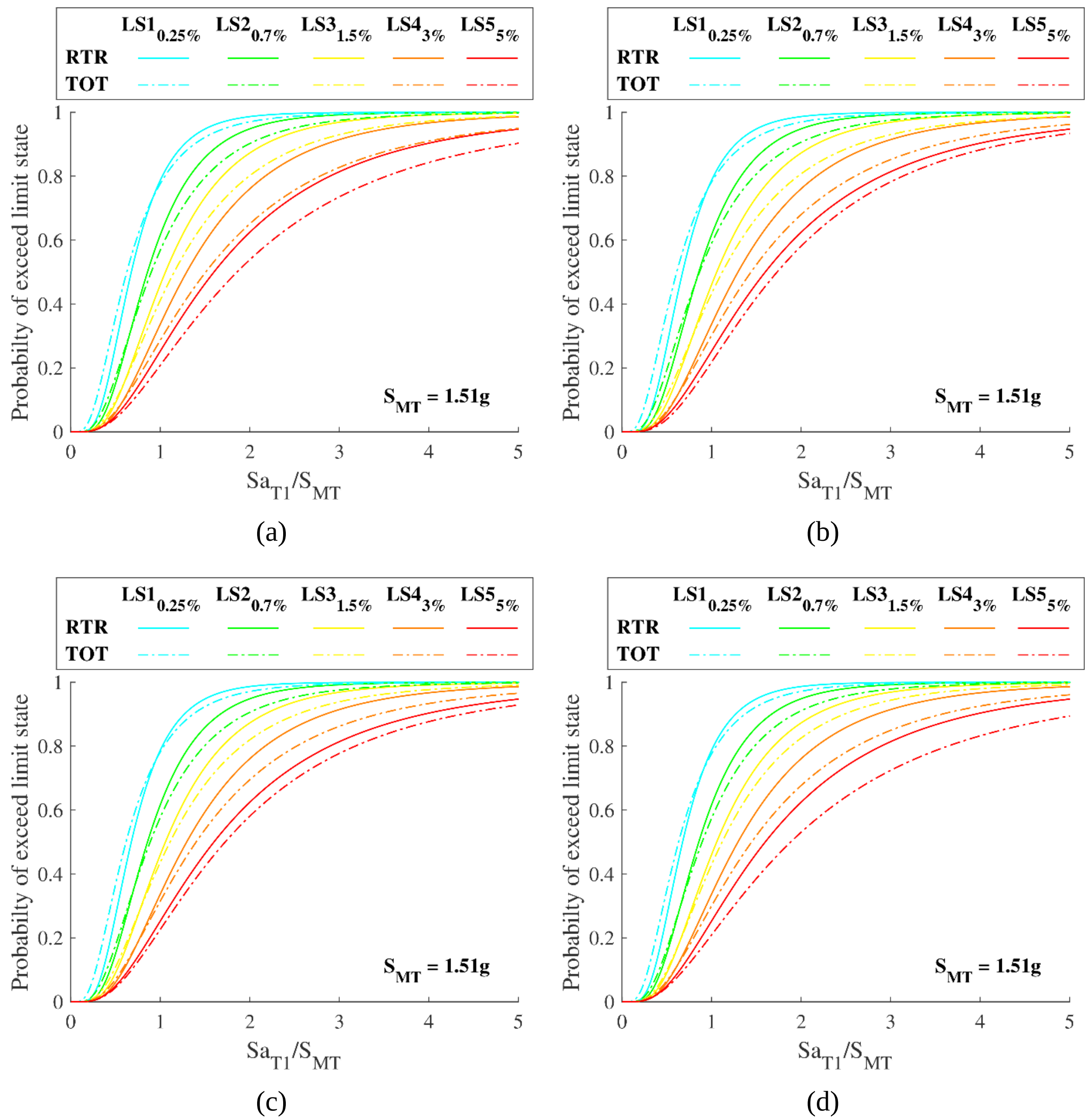

Figure 6.5 – Change in fragility curves due to the consideration of modeling uncertainty for realization models sampled from (a) correlated empirical distributions, (b) uncorrelated empirical distributions, (c) correlated fitted distributions, and (d) uncorrelated fitted distributions

Table 6.5 and Table 6.6 summarize the statistical parameters (median drift intensities and dispersion) associated with each drift-exceedance fragility curve. Figure 6.6 presents the results in terms of ratios that represent the changes in median intensity and dispersion due to the consideration of modeling uncertainty.

Table 6.5 – Median intensities when modeling uncertainty is considered

Drift-based limit state	**$\theta_{SaT1,TOT*}$ E_C[1]**	**$\theta_{SaT1,TOT*}$ E_{NC}[2]**	**$\theta_{SaT1,TOT*}$ F_{DC}[3]**	**$\theta_{SaT1,TOT*}$ F_{NC}[4]**
0.25%	0.95	0.92	0.93	0.95
0.7%	1.36	1.31	1.34	1.35
1.5%	1.74	1.69	1.67	1.69
3%	2.28	2.18	2.11	2.19
5%	2.81	2.62	2.61	2.85

Table 6.6 – Dispersions in analysis variants when modeling uncertainty is considered

Drift-based limit state	**$\beta_{SaT1,TOT*}$ E_C[1]**	**$\beta_{SaT1,TOT*}$ E_{NC}[2]**	**$\beta_{SaT1,TOT*}$ F_{DC}[3]**	**$\beta_{SaT1,TOT*}$ F_{NC}[4]**
0.25%	0.62	0.63	0.62	0.61
0.7%	0.62	0.64	0.62	0.60
1.5%	0.65	0.67	0.64	0.62
3%	0.73	0.70	0.70	0.70
5%	0.76	0.71	0.73	0.78

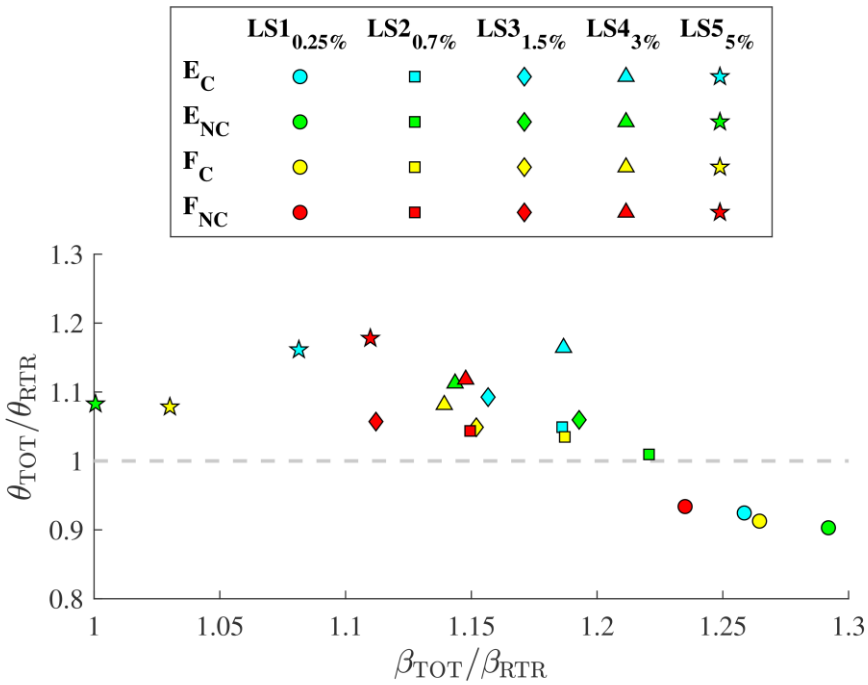

Figure 6.6 – Change in dispersion versus change in median intensities of fragility functions when modeling uncertainty is included

As observed, the consideration of modeling uncertainty increases the dispersion for all drift-based limits states, independently of the variant of analysis. The change in dispersion is shown to be greater at the less severe limit state. The maximum increase, with respect to the case with record-to-record uncertainty only, is 29%, which corresponds to the least severe limit state (0.25% drift threshold). Additionally, modeling uncertainty produces an increase in the median intensities in almost every drift-based limit state. On average, the median drift intensities increase by 5.2%. The exception is identified for the first limit state, where the inclusion of modeling uncertainty produces a decrease of 8.2%. The maximum difference between the variants of analysis is 9.3%, which occur for the most severe limit state. On the other hand, the dispersion increases by 16.2% on average, showing that modeling uncertainty has a greater effect on the latter.

As shown in the fragility curves in Figure 6.5, at the equivalent MCE intensity (Sa_{T1}/S_{MT} = 1.0), the probabilities of exceeding each limit state are on average (i.e. the average of the four variants of analysis) 78%, 58%, 44%, 32%, and 23% for 0.25%, 0.7%, 1.5%, 3%, and 5% drift thresholds, respectively, when modeling uncertainty is included in the analysis. These values are far beyond the performance limits established in ASCE 7, which corresponds to a 10% (or lower) probability of collapse for a ground motion intensity with a 2475 return period.

In terms of the differences produced by the different variant of analysis, the results show that the E_C variant, which corresponds to the case where the strut modeling parameters are sampled from correlated empirical distributions, has the greatest impact on the median drift intensity. On the other hand, the variant where uncorrelated empirical distributions (E_{NC}) are used has on average the greatest impact on the increase of dispersion. The net change (i.e. the maximum difference between the analysis with record-to-record uncertainty only and with the presence of modeling uncertainty) in median drift intensities and dispersions due to the different variant of analysis is 9.2% and 9.9%, respectively. Figure 6.7 illustrates the differences observed among the fragility functions computed based on the results of the different variants of analysis.

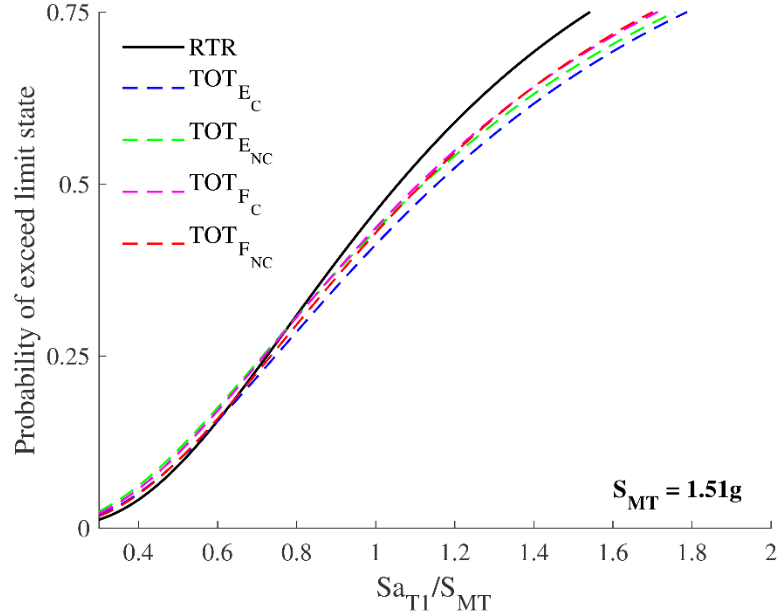

(a)

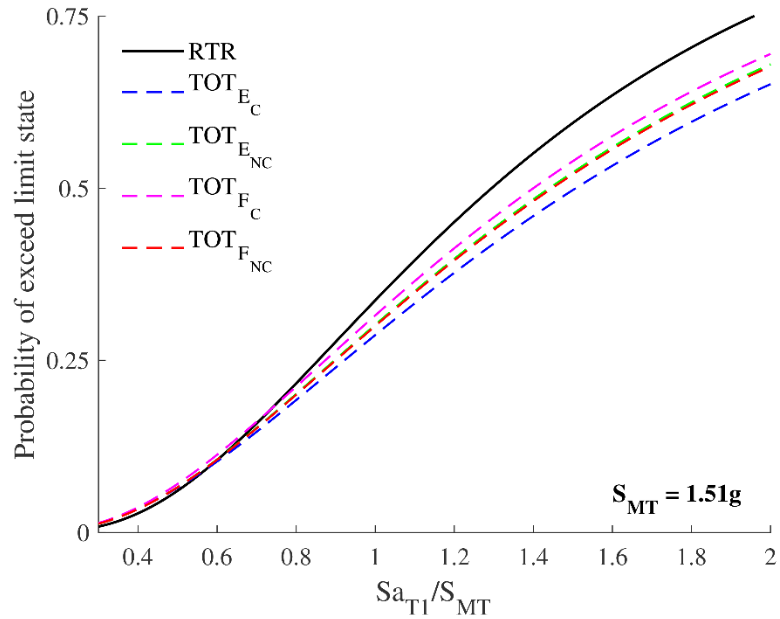

(b)

Figure 6.7 – Differences in the fragility curves for the different variants of analysis. Fragility curves corresponding to limit state with (a) 1.5% and (b) 3% drift thresholds.

6.3 Risk-based assessment

A risk-based assessment of the prototype building is performed to investigate the effects of modeling uncertainties on the mean annual probability of exceeding each of the drift-based limit states. First, the annual rate of exceeding each limit state (λ_{LS}) is computed by integrating the site-specific hazard curve for the prototype building (see Figure 5.7) with the respective drift-exceedance fragility functions. Figure 6.8 illustrates the components required to compute the annual rate of exceedance, which in the case of this study is focused on the SDR_{max} demands.

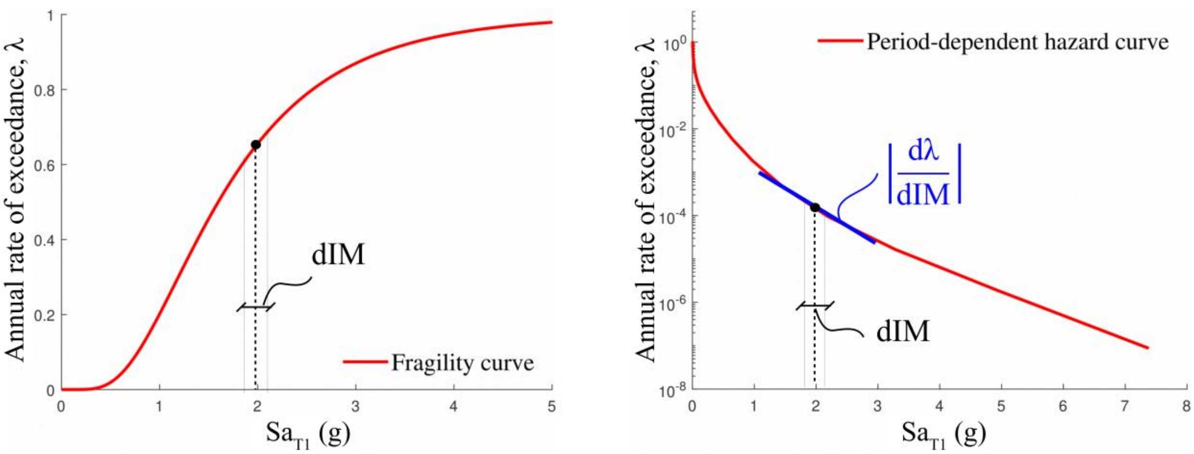

Figure 6.8 – Conceptualization of the calculation for seismic risk assessment

The equation that describe the integration for risk-based assessment procedure is as follows:

$$\lambda_{LS} = \int_{0}^{\infty} \mathrm{P(LS|IM = im)d\lambda(IM)} = \int_{0}^{\infty} \mathrm{P(LS|IM = im)} \left|\frac{\mathrm{d\lambda(IM)}}{\mathrm{dIM}}\right|$$

In the equation above, $P(LS|IM = im)$ denotes the probability of exceeding a certain limit state and is represented by the drift-exceedance fragility functions (left plot in Figure 6.8), and λ represents the seismic hazard function (right plot of Figure 6.8). The integration is made over all the intensity measure (IM) values, which in this study is considered as the spectral acceleration at the fundamental period of the structure (Sa_{T1}). The probability of exceedance of each limit state is computed for 50 years and 100 years, assuming a Poisson distribution. Table 6.7 and Table 6.8 show the limit state probability of exceedance results. The results are shown as probability ratios, in which the probabilities obtained by considering the modeling uncertainties are compared to the probabilities computed based on record-to-record uncertainty only.

Table 6.7 – Change in probabilities of exceeding the drift-based limit states in 50 years due to consideration of modeling uncertainty

$\frac{P_{LS,50ys,TOT}}{P_{LS,50ys,RTR}}$					$P_{LS,50ys,RTR}$
Drift-based limit state	E_C[1]	E_{NC}[2]	F_C[3]	F_{NC}[4]	
0.25%	1.50	1.61	1.54	1.44	0.154
0.7%	1.16	1.32	1.20	1.12	0.096
1.5%	1.07	1.23	1.17	1.07	0.064
3%	1.05	1.06	1.13	1.06	0.046
5%	0.87	0.82	0.90	0.92	0.038

[1] E_C: Using empirical distribution with correlation

[2] E_{NC}: Using empirical distribution without correlation

[3] F_C: Using fitted distribution with correlation

[4] F_{NC}: Using fitted distribution without correlation

Table 6.8 – Change in probabilities of exceeding the drift-based limit states in 100 years due to consideration of modeling uncertainty

$\frac{P_{LS,100years,TOT}}{P_{LS,100years,RTR}}$					$P_{LS,100years,RTR}$
Drift-based limit state	**E_C[1]**	**E_{NC}[2]**	**F_C[3]**	**F_{NC}[4]**	
0.25%	1.44	1.53	1.47	1.39	0.285
0.7%	1.14	1.28	1.17	1.10	0.186
1.5%	1.06	1.22	1.16	1.06	0.125
3%	1.06	1.07	1.13	1.07	0.090
5%	0.88	0.83	0.91	0.92	0.075

[1] E_C: Using empirical distribution with correlation

[2] E_{NC}: Using empirical distribution without correlation

[3] F_C: Using fitted distribution with correlation

[4] F_{NC}: Using fitted distribution without correlation

In terms of the changes in the probabilities of exceeding the drift-based limit sates when modeling uncertainty is considered, the results for the 50 years case are proportionally similar to the results for 100 years. The results shown in Table 6.7 are graphically visualized in Figure 6.9, where the change in the probabilities of exceeding the drift-based limit sates in 50 years due to the consideration of modeling uncertainty are clearly observed at the different limit states.

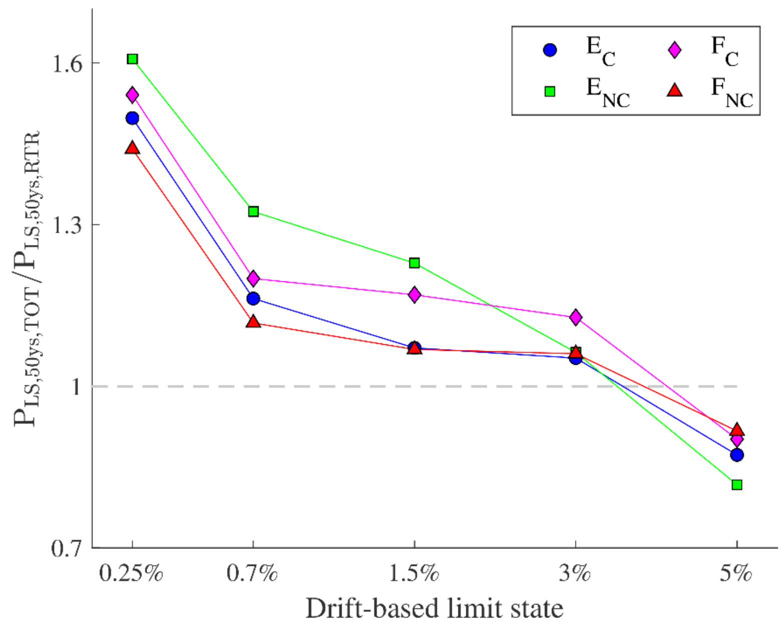

Figure 6.9 – Change in probabilities of exceeding the drift-based limit states in 50 years due to consideration of modeling uncertainty

From the results shown in Table 6.7 and illustrated in Figure 6.9, the probability of exceeding the limit state with threshold at 1.5% drift is about 8% in 50 years. According to empirical evidence (Basha & Kaushik, 2016; Murcia-Delso & Shing, 2012; Stavridis et al., 2012; and others), at this drift demand, it is possible to observe complete collapse of the masonry infill walls. Moreover, this limit state is also a threshold where the strength of the structure starts to degrade and decay rapidly. Therefore, this result provides additional evidence of the seismic vulnerability of this type of structure. The consideration of modeling uncertainty increases on average 13.5% the probability of exceeding the 1.5% drift threshold limit state in 50 years.

The analysis variant E_{NC} has the most significant impact in the probability of exceeding the first three limit states in 50 years, increasing the probabilities by 61%, 32%, and 23%, respectively. In contrast, the analysis variant F_{NC} produces the lowest changes at least in the first four limit states. However, it is worth noting that the maximum difference between the analysis variant that generates the most significant impact and the one that generates the least impact is 17.8% for the second limit state (drift threshold at 0.7%).

6.4 Deaggregation of modeling uncertainty

Deaggregation of the results is carried out in order to evaluate the relative contribution of each of the infill strut modeling parameters on the seismic performance and risk assessment of the prototype building. From the results previously examined, it can be seen that the E_C variant of analysis, where the model realization are sampled based on correlated empirical distributions, reasonably represents the average of the responses of the four variants. In this sense, the disaggregation of the results is evaluated for this variant. The deaggregation is achieved by repeating the same model sampling outlined earlier, but considering the randomness of the strut modeling parameters individually. This means that the model realizations generated using LHS consider only one modeling parameter as a random variables, while the rest are set as the mean values. Then, each model realization is subjected to MSA and the results are grouped depending on the modeling parameter considered as random variable. Figure 6.10 illustrates the changes in median SDR_{max} and dispersion due to the consideration of modeling uncertainty in each infill strut modeling parameter separately.

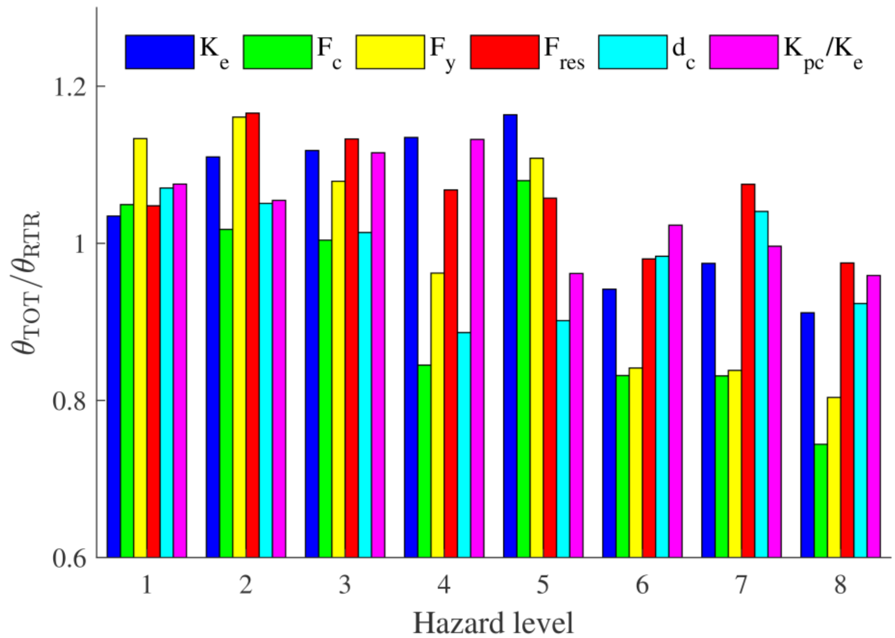

Figure 6.10 – Changes in median SDR_{max} due to the effects of modeling uncertainty included in each parameter separately

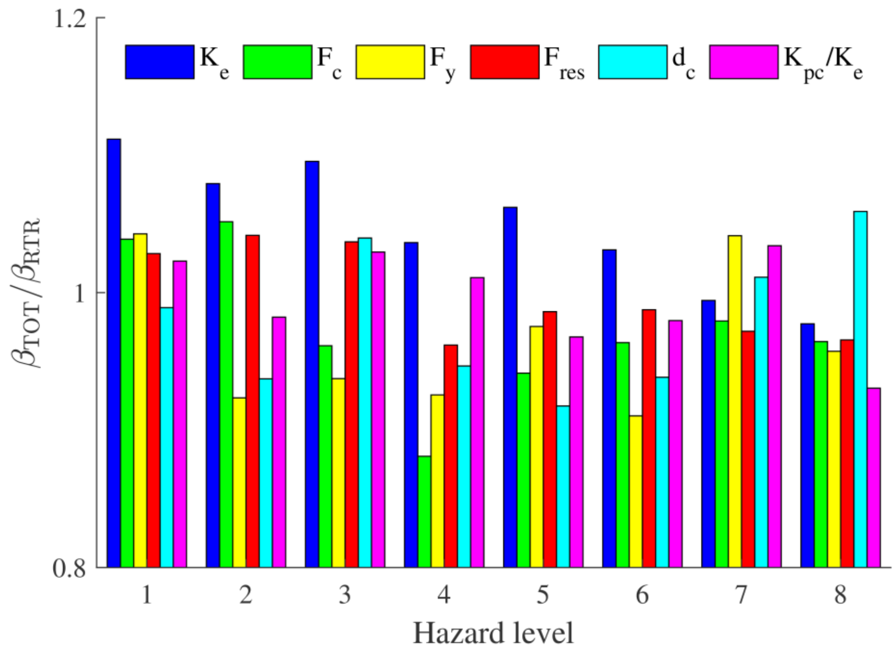

Figure 6.11 – Changes in dispersion of SDR_{max} due to the effects of modeling uncertainty included in each parameter separately

It is observed from Figure 6.10 that the initial stiffness (K_e) has a significant contribution to the change in dispersion for the first three hazard levels. Modeling uncertainty considered in K_e only produces an increase in the dispersion of 11% for hazard level 1 and 9.5% for hazard level 3. On the other hand, the contribution of the capping strength (F_c) and the associated deformation (d_c) to the dispersion tends to be much more negligible with respect to the rest of the modeling parameters. In terms of median SDR_{max}, the results suggest that the two most influential modeling parameters that increase the median SDR_{max} are the strength at yield (F_y) and the residual strength (F_{res}), especially at the first five hazard levels. Figure 6.12 shows the relative contribution of each modeling parameter to the change in the median intensity and the dispersion, for each limit state.

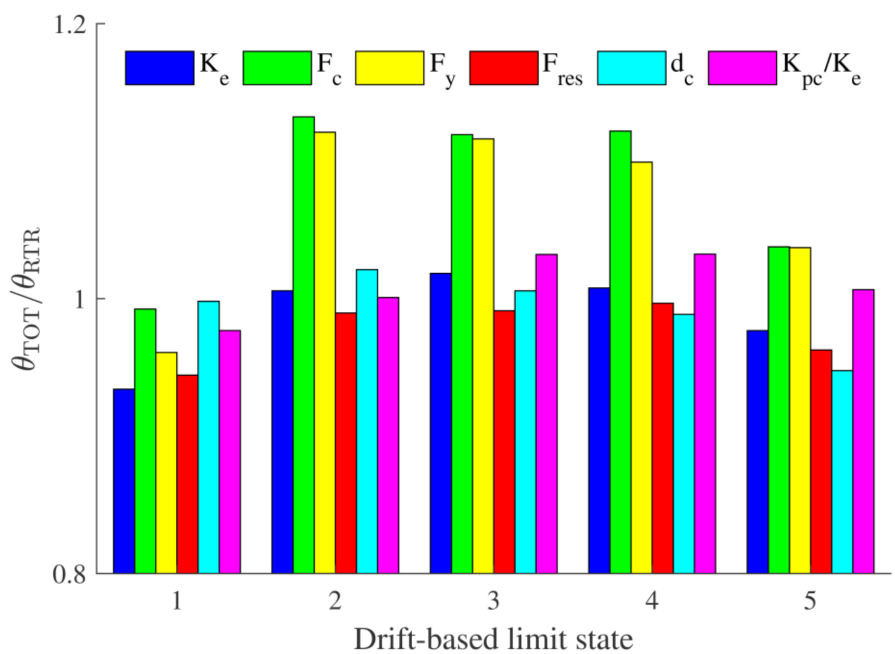

Figure 6.12 – Changes in median drift intensity at each limit state due to the effects of modeling uncertainty considered in each parameter separately

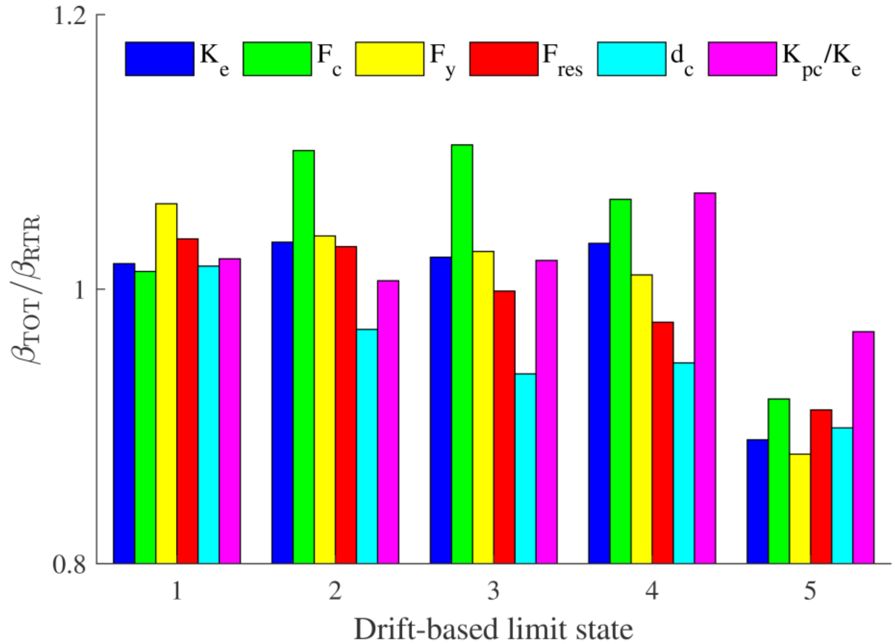

Figure 6.13 – Changes in dispersion of fragility functions at each limit state due to the effects of modeling uncertainty considered in each parameter separately

Consistent with previous results, the relative effect of modeling uncertainty on the drift-exceedance fragility curves is observed to be higher for the limit states with drift thresholds at 0.7%, 1.5%, and 3%. At these limit states, F_c generates the highest increase in both median intensity and dispersion with maximum values of $\beta_{TOT}/\beta_{RTR} = 1.12$ and $\Theta_{TOT}/\Theta_{RTR} = 1.13$. On the other hand, the residual strength (F_{res}) and the post-capping stiffness-to-initial stiffness (K_{pc}/K_e) parameters tend to have a much smaller effect, both in the median intensities and in the dispersions.

Finally, from a risk-based perspective, Figure 6.14 shows the relative contribution of the modeling uncertainty in the change of the probability of exceeding the drift limit states.

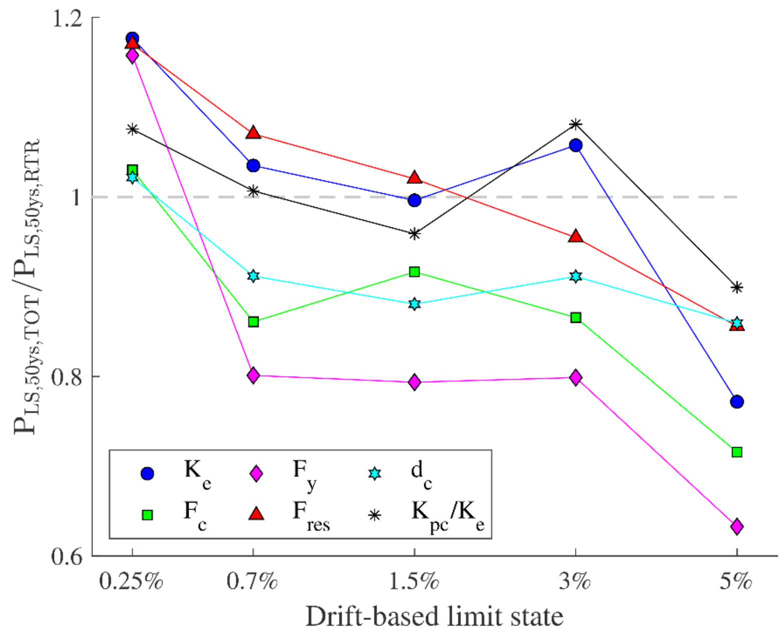

Figure 6.14 – Change in probability of exceeding each limit states in 50 years due to the relative contribution of modeling uncertainty in the infill strut parameters

From Figure 6.14 it can be concluded that, on average, both F_{res} and K_{pc}/K_e have the most significant impact on the probabilities of exceeding the limit state in 50 years. F_{res} governs the increase for the first three limit states, while K_{pc}/K_e controls the results for limit state 4 and 5. The maximum difference occurs at the 5% drift threshold limit state, where the contribution of K_{pc}/K_e is 43% higher than the contribution of F_y.

Chapter 7

Conclusions

The analysis of structures is often conducted with deterministic models, which are intended to represent the mean or expected behavior of the structure. However, several sources of uncertainty have been recognized in structural analysis to have significant impacts on their seismic response and performance. The quantification of uncertainties remains a major challenge in seismic performance assessment of structures. This is particularly relevant for uncertainties related to structural models (modeling uncertainty). Therefore, it is essential to continue strengthening the characterization and communication of the uncertainties involved in seismic and structural analysis.

In this thesis, the focus is on the characterization of the modeling uncertainty embedded in the equivalent strut model used to represent the in-plane nonlinear behavior of masonry infill walls, and the quantification of its effect on the seismic performance of a non-ductile infilled frame structure. Modeling uncertainty is considered at level (ii) epistemic uncertainty according to Bradley (2013), where the six constitutive parameters that define the backbone curve of the equivalent strut model are considered as random variables. Correlated and uncorrelated probabilistic distributions are defined for each strut modeling parameter based on the deduced-to-predicted ratios obtained from (1) experimental data of more than hundred infilled frame specimens and (2) the predictive equations developed by Huang et al. (2020). Modeling uncertainty is examined in conjunction with the variability in the selected ground motions (RTR: record-to-record uncertainty). The quantification of modeling uncertainty is done by conducting a seismic performance assessment on the non-ductile reinforced concrete infilled frame structure studied by Stavridis (2009). Using hazard-consistent ground motions, multiple stripe analysis is performed on randomized nonlinear model realizations of the case study building, generated using Latin hypercube sampling. The effect of modeling uncertainty on the seismic performance of the case study building is investigated in terms of (1) distributions of maximum story drift ratios obtained at different hazard levels and (2) fragility curves associated with drift-based limit states.

The probability distributions defined for each constitutive parameter of the infill strut model and the approach used to quantify the modeling uncertainty and its effects on the seismic performance of masonry infilled frame buildings, could serve as a benchmark to identify vulnerabilities in other similar buildings, for which retrofit plans could be proposed.

The results from the analyses indicate that modeling uncertainty has a significant impact on the maximum drift demands and fragility parameters. At hazards up to 2% probability of exceedance in 50 years, modeling uncertainties have more significant effects, increasing both the median SDR_{max} and the dispersion. In terms of fragility function parameters, modeling uncertainty shifts the median intensities of each limit state on average 6% and increases the dispersion by 18%.

For a ground motion intensity with a 2% probability of exceedance in 50 years, a 26% of probability of exceeding the collapse threshold (i.e. SDR_{max} greater than 5%) is obtained, which is increased to approximately 36% for the most severe hazard level. This is unacceptable according to modern building codes and performance criteria.

The mean annual rate of exceeding the drift-based limit states is obtained from the integration of the drift-based fragility functions with the site-specific hazard curve for the case study building. For a 50 years period, when modeling uncertainty is included, a 60% and 14% probability of exceedance is obtained for the drift-based limit state thresholds where diagonal/sliding shear cracking and collapse of the infill walls is expected, respectively.

In terms of dispersion, the correlated and uncorrelated variants of analysis did not result in a significant difference for both the SDR_{max} distributions and fragility functions. The maximum difference, which occurs for the least severe drift-based limit state, results in approximately 10%. In general, the uncorrelated variants of analysis are observed to have a higher impact on the median measures (i.e. median SDR_{max} and median drift intensity).

From the deaggregation of the effects of modeling uncertainty, it is shown that the initial stiffness (K_e), which is controlled by the elastic modulus (E_m), the thickness (t_w), and the aspect ratio of the masonry wall (h_w/l_w) according to Huang et al. (2020), is the most preponderant contributor to the increase in the dispersion of SDR_{max}. The initial stiffness is 7% more preponderant than the average of the other five strut modeling parameters overall. The capping strength (F_c) is observed to produce on average the highest impact on the dispersion of the drift-based fragility functions. In contrast, the deformation at capping strength (d_c) tends to be the most significant parameter in the decreasing of the dispersion of the fragility functions. For the case of median measures, no clear predominance of any of the six modeling parameters is identified.

7.1 Limitations and future work

In this study, the seismic performance assessment is conducted using a two-dimensional model of the prototype and with concentrated plasticity. As such, it is only possible to evaluate up to level (ii) epistemic uncertainty as defined by Bradley (2013). Future work could investigate the influences of modeling uncertainties at level (i) (i.e. variability in material properties, mass, loads, etc.), and even at level (iii) by using other modeling approaches different from the one used in this study. Moreover, in order to generalize the observations obtained from this study, additional analyses need to be performed on different configurations of this type of structure (i.e. with openings at the infill walls, with bare frames at specific levels, etc.).

The main challenge is the characterization of the modeling uncertainty, which requires experimental data. Therefore, it is essential to conduct new experimental programs in order to better understanding the behavior of this type of structure.

References

Adukadukam, A., Sengupta, A.K. Equivalent strut method for the modelling of masonry infill walls in the nonlinear static analysis of buildings. J. Inst. Eng. India Ser. A 94, 99–108 (2013). https://doi.org/10.1007/s40030-013-0042-y

American Society of Civil Engineers. (2017). Minimum design loads and associated criteria for buildings and other structures: ASCE/SEI 7-16.

Baker, J. W. (2015). Efficient analytical fragility function fitting using dynamic structural analysis. *Earthquake Spectra*, *31*(1), 579–599. https://doi.org/10.1193/021113EQS025M

Baker, J. W., & Cornell, C. A. (2006). Spectral shape, epsilon and record selection. *Earthquake Engineering and Structural Dynamics*, *35*(9), 1077–1095. https://doi.org/10.1002/eqe.571

Baker, J. W., & Lee, C. (2018). An improved algorithm for selecting ground motions to match a conditional spectrum. *Journal of Earthquake Engineering*, *22*(4), 708–723. https://doi.org/10.1080/13632469.2016.1264334

Basha, S. H., & Kaushik, H. B. (2016). Behavior and failure mechanisms of masonry-infilled RC frames (in low-rise buildings) subject to lateral loading. *Engineering Structures*, *111*, 233–245. https://doi.org/10.1016/j.engstruct.2015.12.034

Bradley, B. A. (2013). A critical examination of seismic response uncertainty analysis in earthquake engineering. *Earthquake Engng Struct. Dyn.* https://doi.org/10.1002/eqe.2331 OPINION

Burton, H., & Deierlein, G. (2014). Simulation of Seismic Collapse in Nonductile Reinforced Concrete Frame Buildings with Masonry Infills. Journal of Structural Engineering-asce, 140.

Calvi, G. M., Bolognini, D., & Penna, A. (2004). Seismic performance of masonry-infilled R.C. Frames: Benefits of slight reinforcements. *6th Portoguese Congress on Seismology and Earthquake Engineering*, 253–276.

Campbell, K. W., & Bozorgnia, Y. (2014). NGA-West2 ground motion model for the average horizontal components of PGA, PGV, and 5% damped linear acceleration response spectra. *Earthquake Spectra*, *30*(3), 1087–1114. https://doi.org/10.1193/062913EQS175M

Celarec, D., & Dolšek, M. (2013). The impact of modelling uncertainties on the seismic performance assessment of reinforced concrete frame buildings. *Engineering Structures, 52*, 340–354. https://doi.org/10.1016/j.engstruct.2013.02.036

Chiou, B. S. J., & Youngs, R. R. (2014). Update of the Chiou and Youngs NGA model for the average horizontal component of peak ground motion and response spectra. *Earthquake Spectra*, *30*(3), 1117–1153. https://doi.org/10.1193/072813EQS219M

Choudhury, T., & Kaushik, H. B. (2019). Treatment of uncertainties in seismic fragility assessment of RC frames with masonry infill walls. *Soil Dynamics and Earthquake Engineering*, *126*(July), 105771. https://doi.org/10.1016/j.soildyn.2019.105771

Dolšek, M. (2009). Incremental dynamic analysis with consideration of modeling uncertainties. Earthquake Engineering & Structural Dynamics, 38, 805-825.

Dolšek, M. (2012). Simplified method for seismic risk assessment of buildings with consideration of aleatory and epistemic uncertainty. *Structure and Infrastructure Engineering*, *8*(10), 939–953. https://doi.org/10.1080/15732479.2011.574813

Dolšek, M., & Fajfar, P. (2008). The effect of masonry infills on the seismic response of a four storey reinforced concrete frame-a probabilistic assessment. *Engineering Structures*, *30*(11), 3186–3192. https://doi.org/10.1016/j.engstruct.2008.04.031

Elwood, K. J. (2004). Modelling failures in existing reinforced concrete columns. *Canadian Journal of Civil Engineering*, *31*(5), 846–859. https://doi.org/10.1139/L04-040

Fox, C. R., & Ulkumen, G. (2011). Distinguishing two dimensions of uncertainty. *Perspectives on Thinking, Judging, and Decision Making*, 21–35.

Giovanis, D.G., Fragiadakis, M. & Papadopoulos, V. Epistemic uncertainty assessment using Incremental Dynamic Analysis and Neural Networks. Bull Earthquake Eng 14, 529–547 (2016). https://doi.org/10.1007/s10518-015-9838-7

Gokkaya, B and Baker, JW and Deierlein, G. (2020). *Seismic Reliability Assessment of Structures Incorporating Modeling Uncertainty and Implications for Seismic Collapse Safety* (Issue May). https://purl.stanford.edu/gj011qz6654

Gokkaya, B. U., Baker, J. W., & Deierlein, G. G. (2017). Estimation and impacts of model parameter correlation for seismic performance assessment of reinforced concrete structures. *Structural Safety*, *69*, 68–78. https://doi.org/10.1016/j.strusafe.2017.07.005

Haselton, C. B., Liel, A. B., Taylor-Lange, S. C., & Deierlein, G. G. (2016). Calibration of model to simulate response of reinforced concrete beam-columns to collapse. *ACI Structural Journal*, *113*(6), 1141–1152. https://doi.org/10.14359/51689245

Holmes, M. (1961). Steel frames with brickwork and concrete infilling. *Proc. Inst Civil Eng.*, *6501*, 473–478. https://doi.org/10.1680/iicep.1961.11305

Huang, H., Burton, H. V., & Sattar, S. (2020). Development and utilization of a database of infilled frame experiments for numerical modeling. *Journal of Structural Engineering (United States)*, *146*(6), 1–17. https://doi.org/10.1061/(ASCE)ST.1943-541X.0002608

Ibarra, L. F., Medina, R. A., & Krawinkler, H. (2005). Hysteretic models that incorporate strength and stiffness deterioration. *Earthquake Engineering and Structural Dynamics*, *34*(12), 1489–1511. https://doi.org/10.1002/eqe.495

Jalayer, F., & Cornell, C. A. (2009). Alternative non-linear demand estimation methods for probability-based seismic assessments. *Earthquake Engineering and Structural Dynamics*, *38*(8), 951–972. https://doi.org/10.1002/eqe.876

Jalayer, F., Iervolino, I., & Manfredi, G. (2010). Structural modeling uncertainties and their influence on seismic assessment of existing RC structures. *Structural Safety*, *32*(3), 220–228. https://doi.org/10.1016/j.strusafe.2010.02.004

Kamai, R., Abrahamson, N. A., & Silva, W. J. (2014). Nonlinear horizontal site amplification for constraining the NGA-West2 GMPEs. *Earthquake Spectra*, *30*(3), 1223–1240. https://doi.org/10.1193/070113EQS187M

Krawinkler, H., & Deierlein, G. G. G. (2014). Challenges towards achieving earthquake resilience through performance-based earthquake engineering. In M. Fischinger (Ed.), *Performance-Based Seismic Engineering: Vision for an Earthquake Resilient Society* (Vol. 32, pp. 3–23). Springer, Dordrecht. https://doi.org/https://doi.org/10.1007/978-94-017-8875-5_1

Krawinkler, H., Medina, R. A., & Alavi, B. (2003). Seismic drift and ductility demands and their dependence on ground motions. *Engineering Structures*, *25*(5), 637–653. https://doi.org/10.1016/S0141-0296(02)00174-8

Liel, A. B., Haselton, C. B., Deierlein, G. G., & Baker, J. W. (2009). Incorporating modeling uncertainties in the assessment of seismic collapse risk of buildings. *Structural Safety*, *31*(2), 197–211. https://doi.org/10.1016/j.strusafe.2008.06.002

Lowes, L. N., Mitra, N., & Altoontash, A. (2003). A beam-column joint model for simulating the earthquake response of reinforced concrete frames. *Pacific Earthquake Engineering Research Center, University of California*, *August*, 69.

Masi, A. (2003). Seismic vulnerability assessment of gravity load designed R/C frames. *Bulletin of Earthquake Engineering*, *1*(3), 371–395. https://doi.org/10.1023/B:BEEE.0000021426.31223.60

Mehrabi, A. B., Shing, B. P., Schuller, M. P., & Noland, J. L. (1996). Experimental evaluation of masonry-infilled RC frames. *Journal of Structural Engineering*, *89*(3), 228–237.

Morandi, P., Hak, S., & Magenes, G. (2014). In-plane experimental response of strong masonry infills. *Proc. 9th International Masonry Conference*, 1–12. https://bib.irb.hr/prikazi-rad?rad=712946

Murcia-Delso, J., & Shing, P. B. (2012). Fragility Analysis of Reinforced Masonry Shear Walls. *Earthquake Spectra*, *28*(4), 1523–1547. https://doi.org/10.1193/1.4000075

McKenna, F., Fenves, G. L, and Scott, M. H. (2000) Open System for Earthquake Engineering Simulation. University of California, Berkeley, http://opensees.berkeley.edu.

Sattar, S., Liel, A. B., & Martinelli, P. (2013). Quantification of modeling uncertainties based on the blind prediction contest submissions. *Structures Congress 2013*. https://doi.org/https://doi.org/10.1061/9780784412848.175

Stavridis, A. (2009). Analytical and experimental study of seismic performance of reinforced concrete frames infilled with masonry walls [University of California, San Diego]. In *PhD Thesis*, *University of California*, *San Diego*. https://doi.org/10.1300/J122v22n03_06

Stavridis, A., Koutromanos, I., & Shing, P. B. (2012). Shake-table tests of a three-story reinforced concrete frame with masonry infill walls. *Earthquake Engineering and Structural Dynamics*, *41*(6), 1089–1108. https://doi.org/10.1002/eqe.1174

Stavridis, A., & Shing, B. P. (2015). *Analysis of Seismic Response of Masonry - Infilled RC Frames through Collapse Analysis of Seismic Response of Masonry - Infilled RC Frames through Collapse P . Benson Shing and Andreas Stavridis Synopsis :*

Ugurhan, B., Baker, J. W., & Deierlein, G. G. (2013). Incorporating model uncertainty in collapse reliability assessment of buildings. *Safety, Reliability, Risk and Life-Cycle Performance of Structures and Infrastructures - Proceedings of the 11th International Conference on Structural Safety and Reliability, ICOSSAR 2013, 2005*, 2171–2178. https://doi.org/10.1201/b16387-316

Vamvatsikos, D., & Fragiadakis, M. (2010). Incremental dynamic analysis for estimating seismic performance sensitivity and uncertainty. *Earthquake Engng Struct. Dyn.*, *39*, 141–163. https://doi.org/10.1002/eqe.935

Vořechovský, M., & Novák, D. (2003). Statistical correlation in stratified sampling. *ICAPS 9 Proceedings of International Conference on Applications of Statistics and Probability in Civil Engineering*, 119–124.